

Mineralogy and Geochemistry of Immature Lateritic Crusts developed from Granitoids and Cr-Ni-Bearing Ultramafic Rocks in Southeastern Carajás/Brazil

Marcondes Lima da COSTA^{1*}, Rayara do Socorro Souza da SILVA¹, Elaine de Oliveira MENEZES¹ & Roberto DALL' AGNOL²

¹ Applied Mineralogy and Geochemistry Group (GMGA) – Geology Faculty – Geosciences Institute – Federal University of Pará (mlc@ufpa.br, marcondeslc@gmail.com)

² Technology Institute Vale – ITV

Abstract. Lateritic formations with iron crusts are very frequent in the Amazon region (Brazil). They, in addition to their great importance in containing a large part of the most voluminous ores (iron, manganese, bauxite and kaolin), may be valuable proxies for paleoclimatic reconstitution. In the Carajás region, the oldest lateritic formations are well represented on the high surface (plateaus) and the youngest on the low landscape. The latter have practically not yet been investigated, unlike those of the plateaus, and, considering their paleoenvironmental importance, we carried out a chemical-mineral characterization and geochemical discussion of these crusts (massive, nodular and with lithorelics) sampled in the geological domains of Canaã and Rio Maria. They were analyzed by optical microscopy, XRD, SEM/EDS and whole chemistry. The main minerals are hematite, goethite, kaolinite, quartz, chromite and possibly anatase. SiO_2 , Fe_2O_3 and Al_2O_3 are the main chemical constituents. These data, along with the trace and rare earth element concentrations and associations, allowed us to conclude that the crusts were derived from both granitoids and mafic-ultramafic rocks (high Cr-Ni). The textures and domains of goethite in these crusts can correlate them to the immature lateritic profiles of the Amazon, which formed during the Miocene-Pliocene and partially weathered in the Pleistocene under a hot and humid climate. Since these crusts occupy the Carajás plateaus developed over mature lateritic crusts, they have been formed after the partial denudation of this high land, which exposed the rocky and saprolite under a dry to subarid climate, and then a hot and humid climate was established in that area, promoting the immature lateritic formation, in which the crusts represent its upper portion.

Keywords: Hematite, goethite, chromium, nickel, rare earth elements; granodiorites.

Resumo. MINERALOGIA E GEOQUÍMICA DE CROSTAS LATERÍTICAS IMATURAS DISCRIMINANDO GRANITÓIDES E ROCHAS ULTRAMÁFICAS A CR-NI NO SUDESTE DE CARAJÁS/BRASIL. Formações lateríticas com crostas ferruginosas são muito frequentes na Amazônia. Elas, além de sua importância por conterem grande parte dos minérios mais volumosos (ferro, manganês, bauxita e caolim) da região e País, podem ser valiosos registros para reconstituição paleoclimática. Na região de Carajás, as formações lateríticas mais antigas estão bem representadas nos platôs e as mais jovens nos terrenos mais baixos. Estas últimas praticamente ainda não foram investigadas, ao contrário daquelas dos platôs, e, considerando sua importância paleoambiental, esta pesquisa foi desenvolvida visando sua caracterização químico-mineral e discussão geoquímica. Amostras de crostas ferruginosas (maciças, nodulares e com litorelictos) dessa região foram coletadas nos domínios geológicos de Canaã e Rio Maria e analisadas por microscopia ótica, DRX, MEV / EDS e química total. Os principais minerais são hematita, goethita, caulinita, quartzo, além de traços de cromita e anatásio. Consequentemente, SiO_2 , Fe_2O_3 e Al_2O_3 são os principais constituintes químicos. Esses dados, juntamente com as interpretações de elementos traço e terras raras, nos permitiram concluir que as crostas derivaram tanto de granitóides quanto de rochas máfico-ultramáficas (alto Cr-Ni). Todas as características dessas crostas confirmaram sua relação com as formações lateríticas imaturas da Amazônia, formadas durante o Miocene-Pliocene, parcialmente intemperizadas no Pleistoceno já sob clima quente e úmido. Sua paisagem, sugere que após a denudação parcial dos já elevados terrenos de Carajás, rochas sãs e saprolitos foram expostos sob clima seco e semiárido, sendo em seguida afetados por clima quente e úmido que promoveu a formação laterítica imatura, em que as crostas investigadas representam sua porção superior.

Palavras-chave: Hematita, goethita, cromo, níquel, elementos terras raras; granodioritos.

1 Introduction

The lateritic formations result from the intense chemical-mineral alteration of preexisting rocks exposed to the surface of terrains under a hot and humid tropical climate. These conditions occurred throughout the Earth's geological history and still extend to the present day in various regions of the Earth; therefore, they are found almost all over its surface or near-surface. It distinguishes only in terms of quantity and exposure, whether exposed or buried and modified. The literature on this topic is very rich and has intensified over the past 30 years by advancing in regions previously unthinkable for the occurrence of these formations in low and high latitudes (Brazil, Australia, and Central Africa countries) (Nahon, 1991; Costa, 1991; Nahon & Tardy, 1992; Schellmann 1994; Tardy, 1997; Freyssinet *et al.*, 2005).

Brazil, whose land remained largely in paleoclimatic conditions favorable to lateritic weathering, mainly from the Paleozoic in sporadic pulses, has occurrences of these formations in various parts of its territory, with emphasis on the Amazon, which experienced its phase more lavish for the development of laterites or lateritic formations during the Cenozoic. The Amazon has been located in the intertropical zone since the Mesozoic (Tardy *et al.*, 1991) and is rich in lateritic formations, both mature and immature, many of which form important mineral deposits, such as bauxites, iron, nickel, manganese, gold, and phosphates (Costa, 1991; Schellmann, 1994; Kotschoubey *et al.*, 2005; Costa, 2007). Within this region stands out the Carajás Mineral Province and its surroundings, which is known worldwide for its gigantic mineral expression. However, the importance of lateritic formations in the Carajás region, which joke there in every corner, is still unknown, especially in its surrounding lowland, undulating terrain and once dominated by vigorous forest, today for pastures. The present work focused on these ferroaluminous lateritic crusts that emerge in these lowlands in the region of Canaã dos Carajás and Rio Maria to characterize them and from the data obtained, discuss their

possible formation processes and possible parent rocks and discuss climate changes that occurred in the region during their formation and degradation.

2 Materials and methods

2.1 Geological and Physiographic Aspects of the Studied Region

2.1.1 Geological context

The Carajás Mineral Province is the oldest and best represented portion of the Amazonian Craton (Huhn *et al.*, 1988; Dall'Agnol *et al.*, 2006; Oliveira *et al.*, 2006; Fabre *et al.*, 2011; Feio *et al.*, 2013; João, 2013). It comprises the crustal segments Rio Maria Domain (Mesoarchean), to the south, and Carajás Domain (Neoarchean), to the north (Dall'Agnol *et al.*, 2013; Oliveira *et al.*, 2006; Feio *et al.*, 2013) (Figure 1).

The tonalite-trondhjemite-granodiorite (TTG) Lands of Rio Maria (TGGRM) are formed, according to Feio *et al.* (2013), by greenstone belts and by five main groups of granitoids. Three groups, Lagoa Seca, Sapacuaia and Babaçu, constitute the greenstone belts represented by metaultramafic rocks, followed by metabasics and, at the top, by porphyritic metadacites and continental and vulcanochemical metasediments (Souza, 2001). The granitoids are in the oldest TTG Series of Rio Maria: (1) Tonalite Arco Verde and Trondhjemite Mogno (2.96 ± 0.02 Ga), followed by the formation of the Tonalitic Caracol and Tonalite Mariazinha Complex (2.93 ± 0.02 Ga); (2) mainly granodioritic granitoids with high Mg contents (2.87 Ga), formed by Rio Maria granodiorite, intermediate and associated mafic rocks; and (3) leucogranodiorites and calcium-alkaline leucomonzogranites enriched in Ba and Sr, represented by the Guarantã Suite and similar granites (2.87 Ga); and (4) younger TTGs: Trondhjemite Água Fria (2.86 Ga) and (5) potassium leucogranites (2.86 Ga), represented by Xinguara, Mata Surrão granites and similar.

In turn, Canaã dos Carajás is between the southern border of the Carajás Basin and the transition subdomain to the north and

south of the Carajás Domain, respectively. Feio *et al.* (2013) describe that the area is geologically constituted by granitoids and small anorogenic Paleoproterozoic granitic plutons (Rio Branco Granitic Body and similar), on which the occurrences of lateritic crusts are found.

2.1.2 Relief

The study region is located in the relief unit called depression of the southern Amazon, characterized by terrains with a medium to high degree of dissection, represented by low slopes of convex tops that generally assume the shape of a half-orange (Bignelli *et al.*, 1998), with the domain of relatively low altitude, approximately 164 m (Figure 2A).

2.1.3 Soils

The region of this study is comprised of red-yellow dystrophic Argisols (Figura 2B) that reflect the most recent climatic conditions and partly the rocks exposed to weathering agents (Horbe, 1995; Kotschoubey *et al.*, 2005).

Argisols form the second largest soil class in Brazil and occur in approximately 70% of the Carajás Domain (Araújo *et al.*, 1991; Embrapa, 2006). They are acidic soils of low fertility and variable depth that occur in more dissected and rugged reliefs, are quite susceptible to erosion and are frequent in the Amazon region (Araújo *et al.*, 1991; Coelho *et al.*, 2002).

For the development of the present work, field recognition was carried out to evaluate the extension of lateritic crusts in the Canaã dos Carajás, Xinguara and Rio Maria regions, which are better known for their granitoids and granodiorites. On this occasion, 21 samples of lateritic crusts and some outcropping primary rocks were collected.

In the laboratories, the samples were described macroscopically and microscopically with the aid of a binocular magnifying glass and a petrographic microscope with reflected light accompanied by photographic images. Subsequently, they were sprayed for mineralogical and chemical analysis. The mineralogical phases were

identified by means of X-ray diffraction (XRD), scanning electron microscopy (SEM) and dispersive energy spectroscopy (EDS). For XRD analyses, a Bruker D2 PHASER diffractometer was used, with a Cu anode, Lynxeye detector (1D mode); increment of $0.02^{\circ}2\theta$; 0.2 s step time; and 0.1 mm slit operating at 300 W (30 KV and 10 mA) in the angular range from 5° to $75^{\circ}2\theta$. The SEM images were obtained by the detection method of backscattered electrons in the Hitachi TM3000 equipment. The minerals of interest were analyzed using an Oxford Instruments SwiftED3000 energy dispersive system (EDS) with voltage acceleration from 5 to 15 KV and an SDD detector (161 eV Cu-K α) coupled to the SEM. All of these analyses were carried out in the laboratories of the Graduate Program in Geology and Geochemistry (PPGG) of the Institute of Geosciences of the Federal University of Pará (UFPA) and were supported by the ITV Paleoclimate project. The total chemical analyses of selected crust samples were performed at Acme Analytical Laboratories Ltd., with support from ITV-Belem.

3 Results and discussion

3.1 Morphological Aspects of the Lateritic Iron Crusts and Mineralogy

According to their general textural aspects, samples of lateritic crusts from Canaã and Rio Maria were subdivided into massive, nodular crusts and crusts with relic material.

The main minerals identified by XRD are goethite, hematite, kaolinite, and quartz (Figure 3), with inference for anatase. In terms of mineral-forming species, the crusts in general do not show distinctions between them. Chromite was performed in a single sample (Figure 3D).

The massive crusts stand out due to the absence of nodules and are whitish and not very porous (Figure 4A and B). They are presented as a reddish-brown plasma involving domains of quartz and kaolinite (Figure 4C and D).

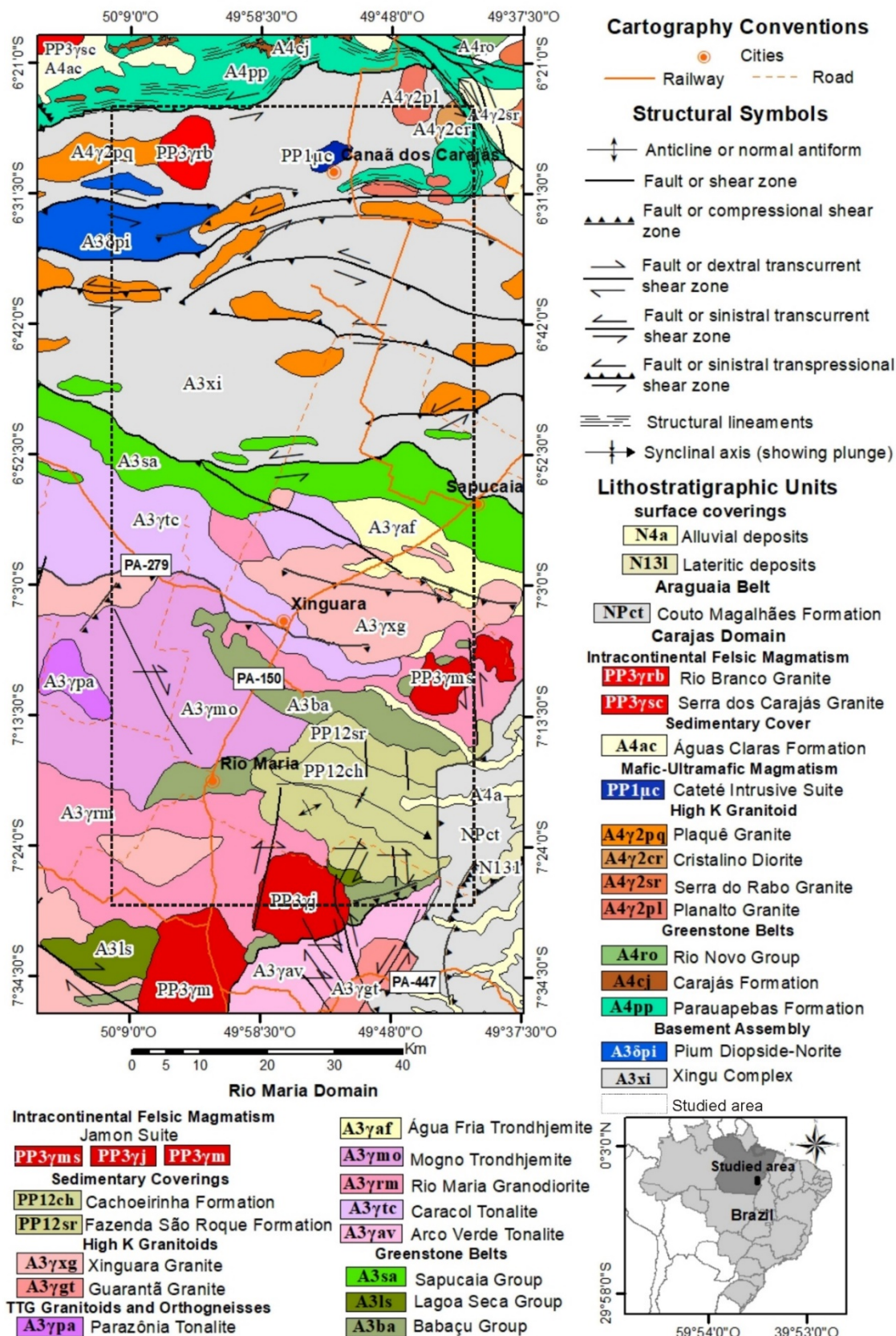


Figure 1. Geological map of the Canaã-Río Maria region. Modified from Vasquez et al. (2008).

Figura 1. Mapa geológico da região Rio Maria-Canaã. Modificado de Vasquez et al. (2008).

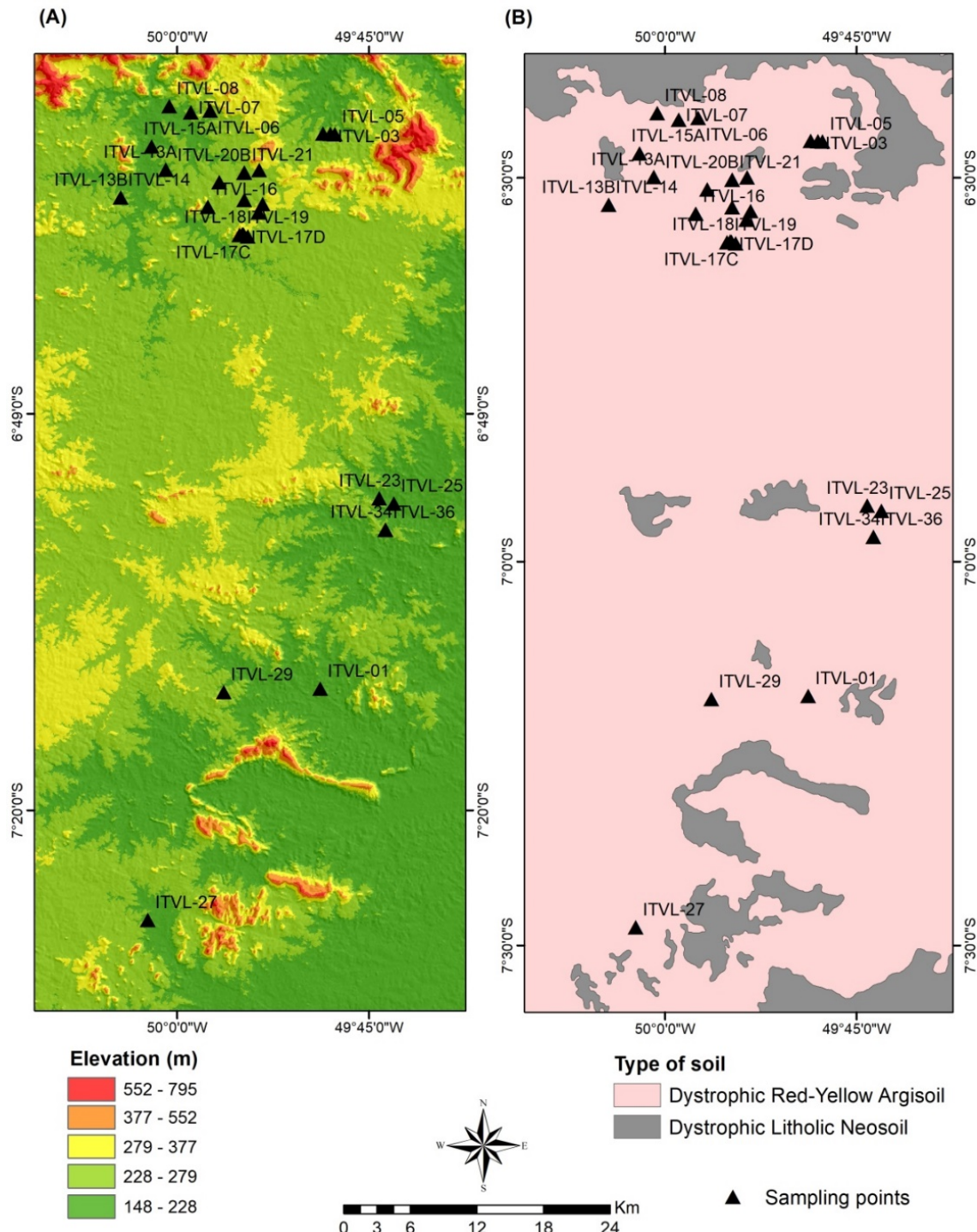


Figure 2. Physiographic aspects of the study area Canaã – Rio Maria: A) Digital elevation model of the region using the Shutter Radar Topography Mission (SRTM) from the USGS Earth Explorer (<https://earthexplorer.usgs.gov/>). Note that the collected sample points are between the minimum and average altitudes. B) Soil map of the region. Modified from IBGE (2008), scale 1: 1800,000.

Figura 2. Aspectos fisiográficos do local de estudo. A) Modelo digital de elevação da região usando o Shutter Radar Topography Mission (SRTM) do USGS Earth Explorer (<https://earthexplorer.usgs.gov/>). Observar que os pontos das amostras coletadas estão entre a altitude mínima e média; B) Mapa de solos da região. Modificado do IBGE (2008). Escala 1:1.800.000.

SEM images and qualitative EDS analyses allowed the identification of barite crystal aggregates and pseudohexagonal kaolinite booklets interspersed with Fe oxyhydroxides, probably goethite/hematite (Figure 4E and F), as well as cryptocrystalline

masses of chalcedony (quartz), sometimes microporous, corroded, and subhedral prismatic crystals (Figure 4G and H). SEM photomicrography and EDS chemical analysis showed that the whitish portion was due to the presence of chalcedony.

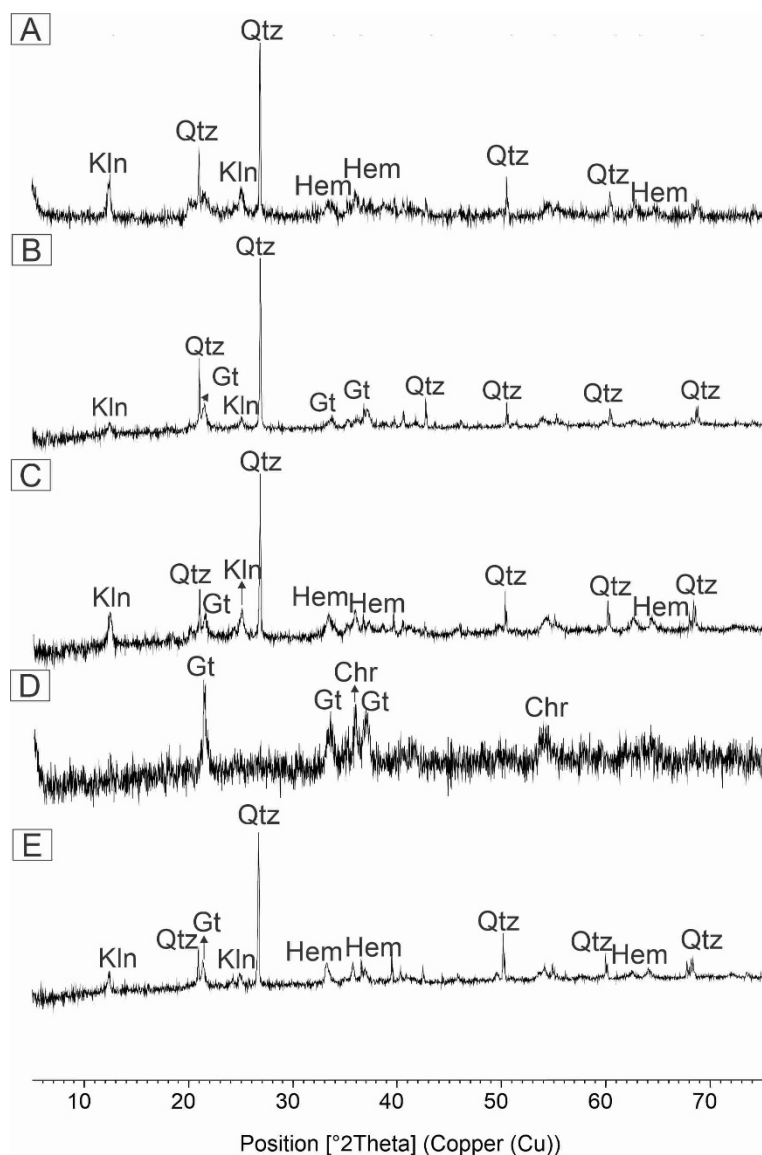


Figure 3. X-ray diffractograms of different lateritic crusts showing their main mineral identified. A) Massive crust; B) Massive crust with chalcedony fragments; C) Nodular crust; D) Nodular crust with chromite; E) Crust with rock relic. Kln = kaolinite, Gt = goethite, Qtz = quartz, Hem = hematite, Chr = chromite.

Figura 3. Difratogramas de raios X das diferentes crostas lateríticas mostrando os principais minerais identificados. A) Crosta maciça; B) Crosta maciça com fragmentos de calcedônia; C) Crosta nodular; D) Crosta nodular com cromita; E) Crosta com relictos de rocha. Kln = caulinita, Gt = goethita, Qtz = quartzo, Hem = hematita, Chr = cromita.

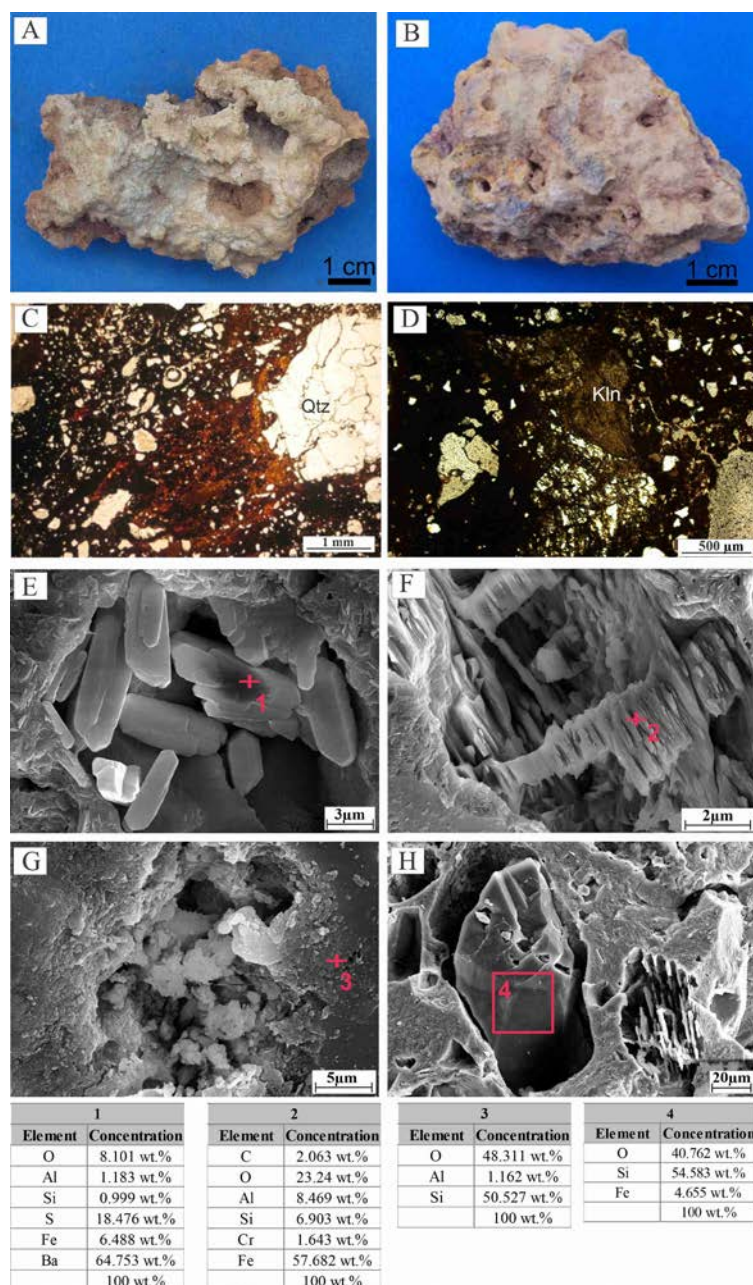


Figure 4. Mesoscopic aspects of the lateritic crusts from the Canaã and Rio Maria regions. A) Massive crust with whitish portions of chalcedony on its surface; B) Massive friable crust, consisting of kaolinite. Photomicrographs of crusts; C) Reddish brown plasma cementing quartz grains; parallel nicols; D) Kaolinite portion inside of the ferruginous matrix; crossed nicols. Qtz: quartz; Kln: kaolinite. SEM images of punctual aspects of crusts and their respective chemical analysis by EDS (Analyses 1, 2, 3 and 4); E) Prismatic barite crystals (EDS analysis 1); F) Kaolinite crystals forming booklets (EDS analysis 2); G) Quartz crystallites in the chalcedony mass (EDS analysis 3) inside the ferruginous crust; H) Chalcedony mass with a quartz crystal (EDS analysis 4) inside a dissolution cavity.

Figura 4. Aspectos mesoscópicos das crostas lateríticas da região de Canaã e Rio Maria. A) Crosta maciça com porções esbranquiçadas de calcedônia em sua superfície; B) Crosta maciça friável, constituída por caulinita. Fotomicrografias de crostas. C) Grãos de quartzo cimentando plasma marrom avermelhado; nicóis paralelos; D) Massa de caulinita na matriz ferruginosa; nicóis cruzados. Qtz: quartzo; Kln: caulinita. Imagens de MEV dos aspectos pontuais das crostas e suas respectivas análises químicas por EDS (Análises 1, 2, 3 e 4); E) Cristais de barita prismáticos (análise EDS 1); F) Cristais de caulinita formando livretos (análise EDS 2); G) Cristalitos de quartzo na massa de calcedônia (análise EDS 3) no interior da crosta ferruginosa; H) Massa de calcedônia com um cristal de quartzo (análise EDS 4) dentro de uma cavidade de dissolução.

The nodular crusts stand out for the domain of nodules of dark brown in color, sometimes in reddish to ochre shades (Figure 5A to F) with cement also of similar color, all dominated by ferruginous material (oxyhydroxides); microcavities are frequent and can be coated with kaolinite and iron oxyhydroxides. The plasma composed of

hematite and goethite encompasses kaolinite and quartz and involves ferruginous nodules with variable contours. Dissolution cavities, many due to micro radicular activities or even dissolving quartz grains trapped during the formation of the crust, are frequent (Figure 5A and B).

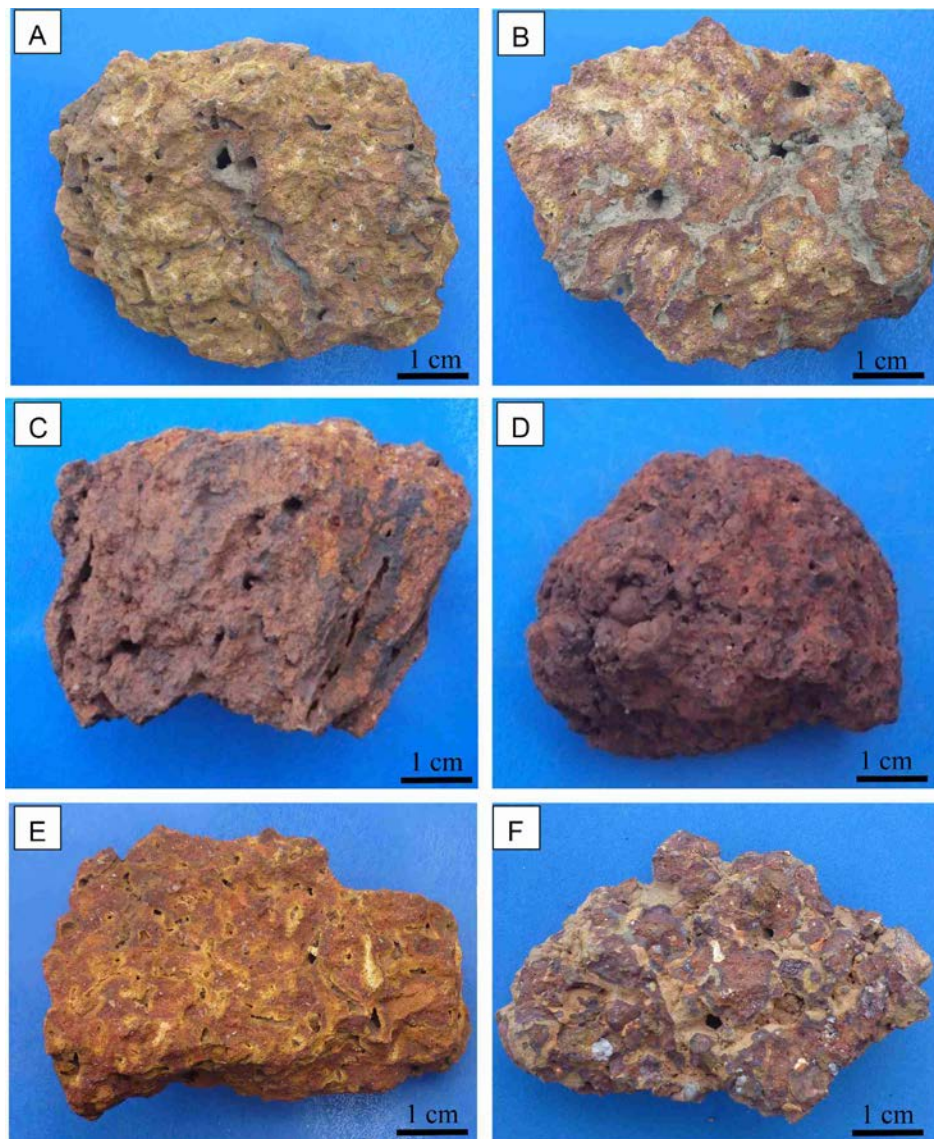


Figure 5. Mesoscopic aspects of nodular crusts from the Canaã and Rio Maria domains. A) and B) Porous crusts in which cavities are formed by alteration and partly infilled by new formation of clayey material; C) and D) Porous crusts with dark portions and cavities coated with dark ferruginous material (in general goethite); E) Porous crust with intertwining of hematitic-goethitic material; F) Nodular crust displaying dark brown cortex around the nodules and some pores.

Figura 5. Aspectos mesoscópicos das crostas nodulares dos domínios Canaã e Rio Maria. A) e B) Crostas porosas nas quais as cavidades são formadas por alteração e parcialmente preenchidas por nova formação de material argiloso; C) e D) Crostas porosas com porções escuas e cavidades revestidas por material ferruginoso escuro (em geral goethita); E) Crosta porosa com entrelaçamento de material hematítico-goethítico; F) Crosta nodular apresentando córtex marrom-escuro ao redor dos nódulos e alguns poros.

Photomicrographs of porous crusts allow the identification of dark and opaque porous nodules composed of iron oxyhydroxides cemented by yellowish ferruginous plasma, probably with kaolinite (Figure 6A and B); a porous iron pisolite strongly digested (Figure 6C); dissolution pores and fractured and/or corroded quartz remnants cemented by iron oxyhydroxide plasma (Figure 6D, E and F); several nodules immersed in a black and porous ferruginous (hematitic domain) in contact with an ochre micromass (goethite, and kaolinite, probably), as indicated by a dotted red line (Figure 6G); a brownish ferruginous nodule partially digested and partially filled by yellowish ferruginous plasma surrounded by black ferruginous plasma (Figure 6H); porous reddish ferruginous plasma describing intraplasmic micronodules (Figure 6I); subspherical nodules in iron oxyhydroxide plasma plenty of micro cavities (Figure 6J). Therefore, porous crusts were distinguished by the presence of intraplasmic micronodules, in black, brown, or yellow, and even red tones. Cement also assumes the same shades. Thus, they demonstrate the dominance of iron oxyhydroxides, represented by hematite and goethite, in addition to kaolinite, according to the XRD data.

Micromorphological aspects after SEM images, such as platy iron oxy-hydroxide aggregates generating botryoid or rosette features, can be observed in the iron-rich nodule matrix (Figure 7A through H) and some EDS chemical analyses (points 1 through 7). In the components that make up part of these images, a marked presence of Cr can be identified (Figure 7H, EDS analysis 7). Kaolinite describes crystal aggregates of nanometric plates and eggshell surfaces (Figure 7A, EDS analysis 1). The uneven intergrowth of nanometer crystals of kaolinite and goethite can also be confirmed (Figure 7B, EDS analyses 2), and the goethite (or hematite) nature of the 3 µm discoid on the goethite-kaolinite botryoidal surface (Figure 7C, EDS analysis 3) was also demonstrated. The domain of platy nanocrystals of hematite and/goethite and kaolinite in the banded ferruginous is also observed in the SEM/EDS analysis (Figure 7D,

EDS analysis 4) and seems to be characteristic. These platy nanocrystals also occur in subspherical and botryoidal aggregates (Figure 7E). Certainly, they correspond to the nodules observed in the optical microscope described in Figure 6. Some spheroids are also clearly formed by platy nanocrystals in rosette aggregates (hematite, probably after crystal morphology) with some kaolinite (Figure 7F, EDS analysis 5). Another textural expression was the presence of hyphal aggregates in the platy domain of iron oxyhydroxide with kaolinite (Figure 7G, EDS analysis 6). The iron oxyhydroxides may present uneven grains, which contain some chromium (Figure 7H, EDS analysis 7), suggesting a possible ultramafic rock contribution.

The crusts with dominant relict material or lithorelicts (Figure 8) are those with mesoscopic fragments of banded iron formation (BIF) (Figure 8A) and of milky quartz (Figure 8B). The typical alternating bands after optical microscopy of iron oxyhydroxides and quartz can be seen in Figure 8C with many more details in Figure 8D. The general color is also brown to dark brown. Under the optical microscope (Figure 8C to H), hematite, goethite and kaolinite cement the quartz grain-likes in the quartz bands of a BIF rock. Evidence of a partly lateritized BIF fragment is indicated in Figure 8E and F), where an iron oxyhydroxide nodule partly substitutes this rock.

Similar to the previous iron crusts, hematite and goethite exhibit nano- and platy crystals associated with kaolinite, in general forming subspherical aggregates (Figure 9A through F). Even on the SEM scale, one can identify the BIF microfragment involved in the newly formed iron oxyhydroxide cement (Figure 9A) with the formation of intraplasmic micronodules (Figure 9B) and reorganization of the iron band with iron oxyhydroxide and kaolinite (Figure 9C, EDS analysis 3). The colloform banded plasma can also be formed only by iron oxyhydroxide (Figure 9D). Here, cross-plastic nanocrystals (most likely hematite and some kaolinite) developing rosettes were also observed (Figure 9E and F, EDS analysis 5).

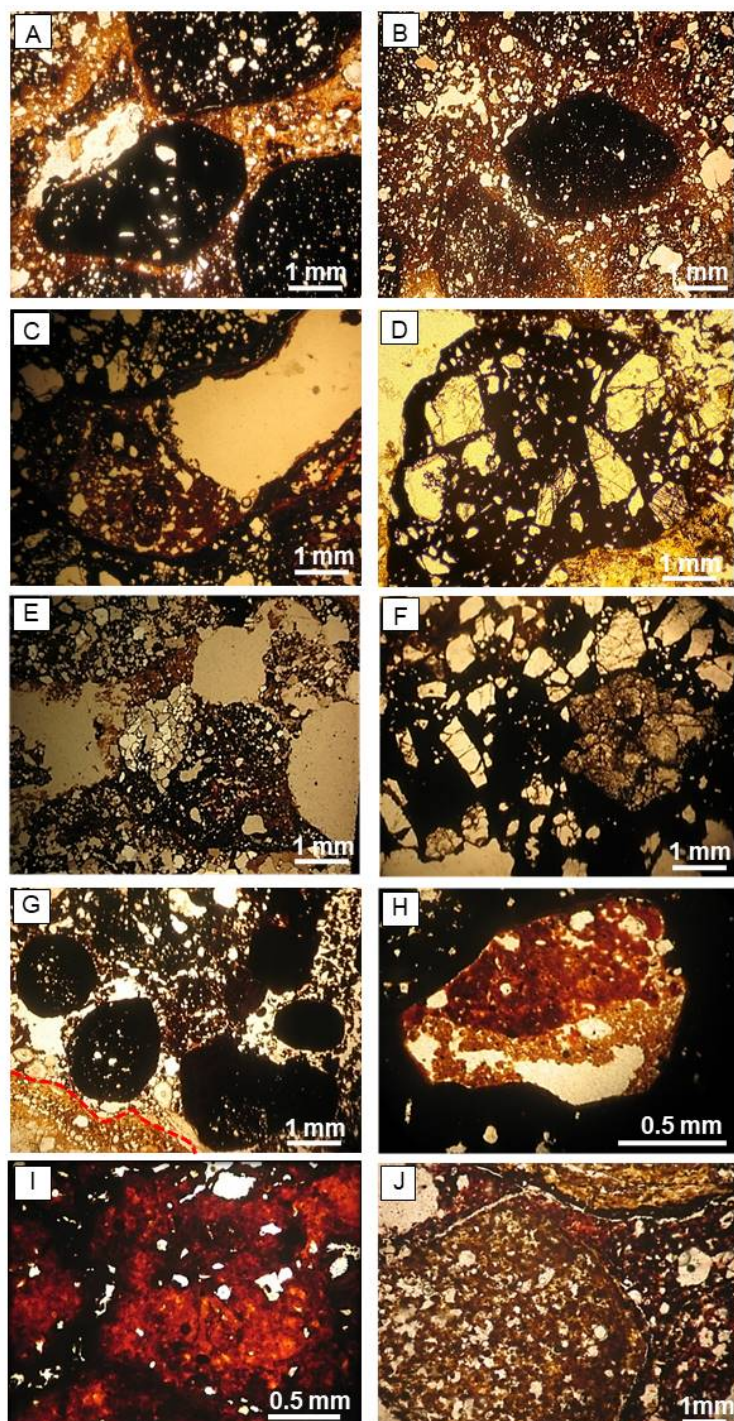


Figure 6. Photomicrographs of porous crusts. A) and B) Porous nodules cemented by ferruginous plasma; C) Iron pisolite partially digested by ferruginous plasma; D), E) and F) Dissolution pores and fractured and/or corroded quartz remnants cemented by iron oxyhydroxide plasma; G) Nodules immersed in ferruginous micromass (hematitic domain) in contact with ochre goethite, as indicated by a dotted red line; H) Nodule partially digested by ferruginous plasma; I) Porous reddish ferruginous plasma; J) Subspherical nodules in iron oxyhydroxide plasma plenty of microcavities. Parallel nicols.

Figura 6. Fotomicrografias de crostas porosas. A) e B) Nódulos porosos cimentados por plasma ferruginoso; C) Pisólito ferruginoso parcialmente digerido por plasma ferruginoso; D), E) e F) Poros de dissolução e relictos de quartzo fraturados e / ou corroídos, cimentados por plasma de oxi-hidróxido de ferro; G) Nódulos imersos em plasma hematítico, em contato com goethita ocre, indicados por linha vermelha pontilhada; H) Nódulo parcialmente digerido por plasma ferruginoso; I) Plasma ferruginoso avermelhado poroso; J) Nódulos subesféricos em plasma de oxi-hidróxido de ferro com abundantes microcavidades. Nicós paralelos.

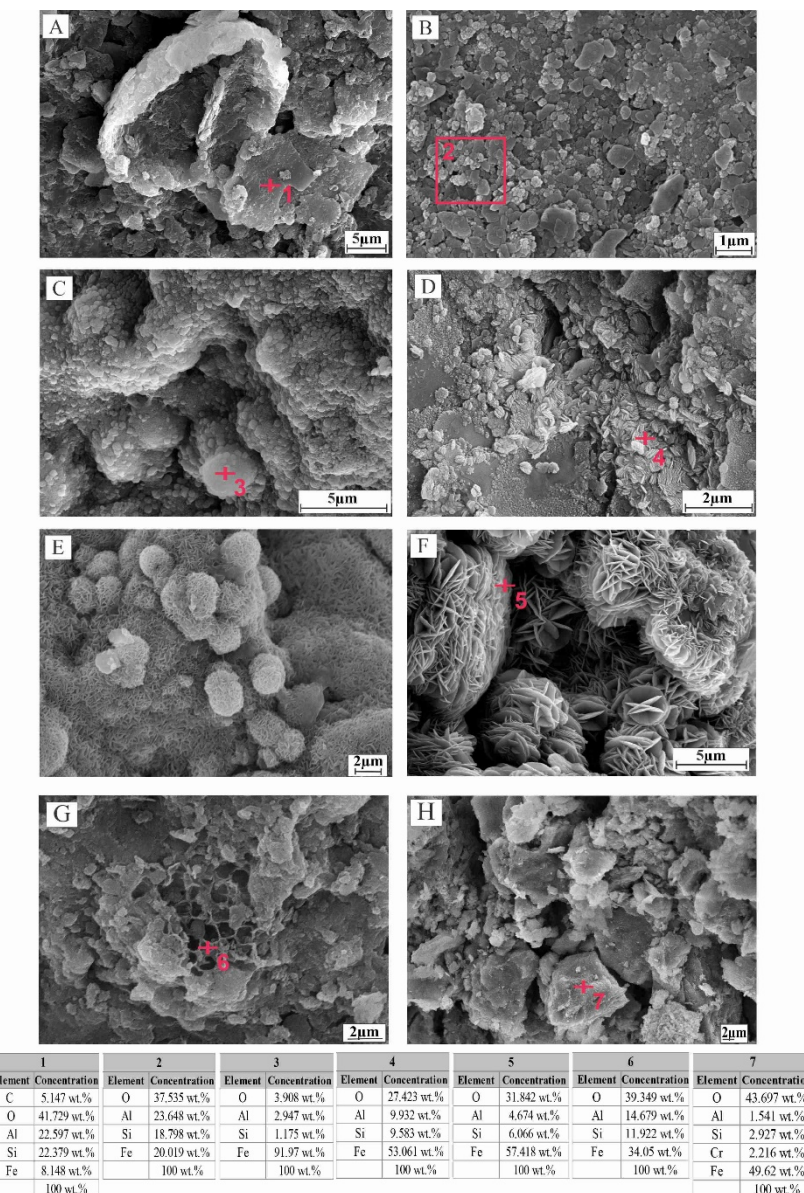


Figure 7. Scanning electron microscopic images showing some micromorphological aspects in the iron rich nodule matrix (A through H) and some EDS chemical analyses (points 1 through 7). A) Aggregates of kaolinite nanometric crystals describing platy and eggshell surfaces (EDS analysis 1); B) Uneven surface described by intergrowth of nanometer crystals of kaolinite and goethite (EDS analyses 2); C) A 3 μm discoid of iron (goethite?) on the goethite-kaolinite botryoidal surface (EDS analysis 3); D) Parallel massive iron rich micro plates partly covered with nanocrystals of hematite and kaolinite (EDS analysis 4); E) Platy nanocrystals of goethite and some kaolinite describing sub spherical and botryoidal aggregates; F) Details of sub spheroids showing the platy crystals (EDS analysis 5); G) Platy and hyphae aggregates of iron oxyhydroxide with kaolinite (EDS analysis 6); H) Distinct morphological aspects of iron oxyhydroxides bearing chromium (EDS analysis 7).

Figura 7. Imagens de microscopia eletrônica de varredura mostrando alguns aspectos micromorfológicos na matriz do nódulo rica em ferro (A a H) e algumas análises químicas EDS (pontos 1 a 7). A) Agregados de cristais nanométricos de caulinita com superfície placosa em padrão casca de ovo (análise EDS 1); B) Superfície irregular com intercrescimento de cristais nanométricos de caulinita e goethita (análises EDS 2); C) Um grande discoide ferruginoso de 3 μm (goethita?) na superfície botrioidal goethita-caulinita (análise EDS 3); D) Micro placas paralelas ricas em ferro maciço parcialmente cobertas com nanocristais de hematita e caulinita (análise EDS 4); E) Nanocristais placosos de goethita e caulinita descrevendo agregados subesféricos e botrioidais; F) Detalhes dos subesferoides mostrando os cristais placosos (análise EDS 5); G) Agregados placosos e hyphae de oxi-hidróxido de ferro com caulinita (análise EDS 6); H) Aspectos morfológicos distintos de oxi-hidróxidos de ferro contendo cromo (análise EDS 7).

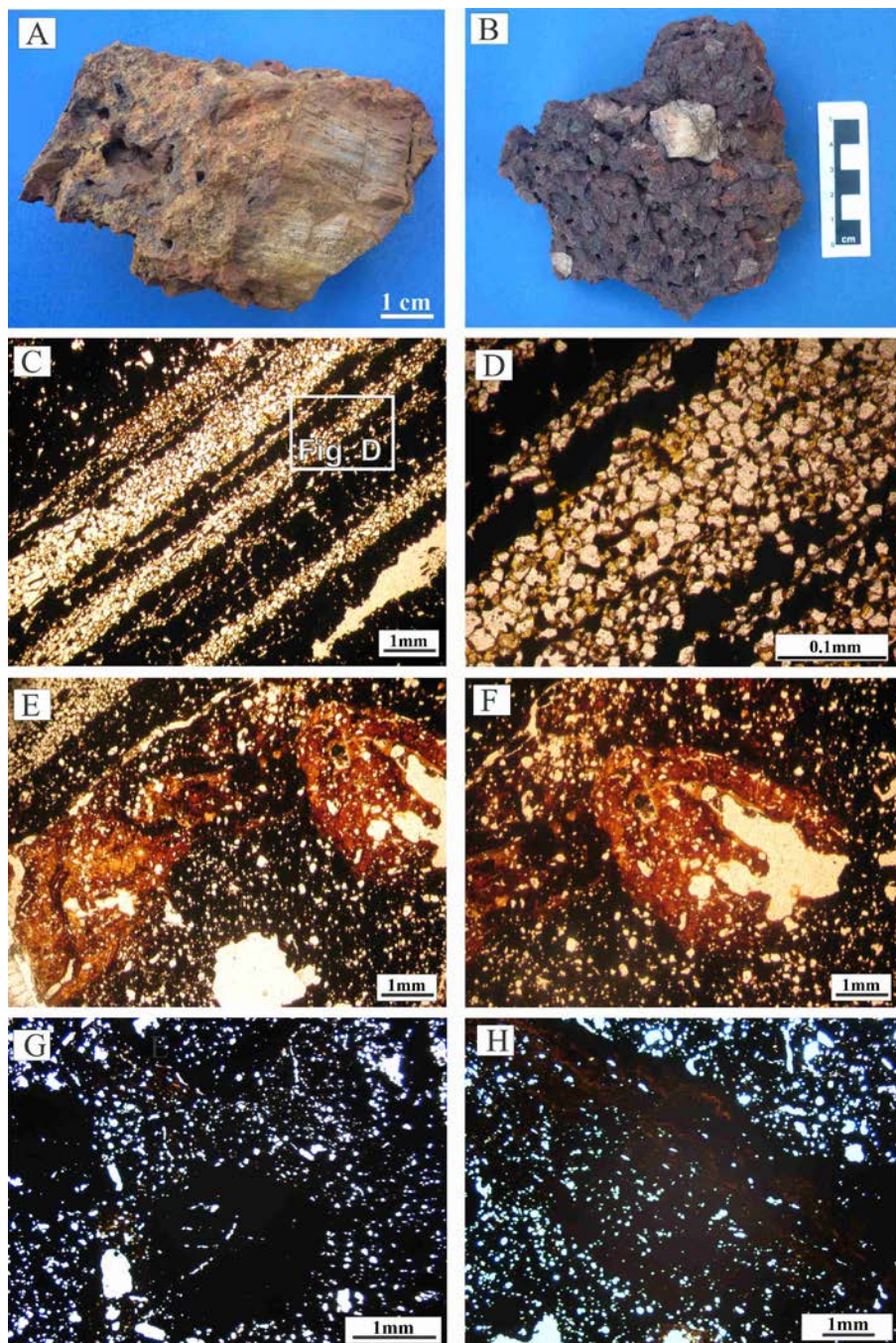
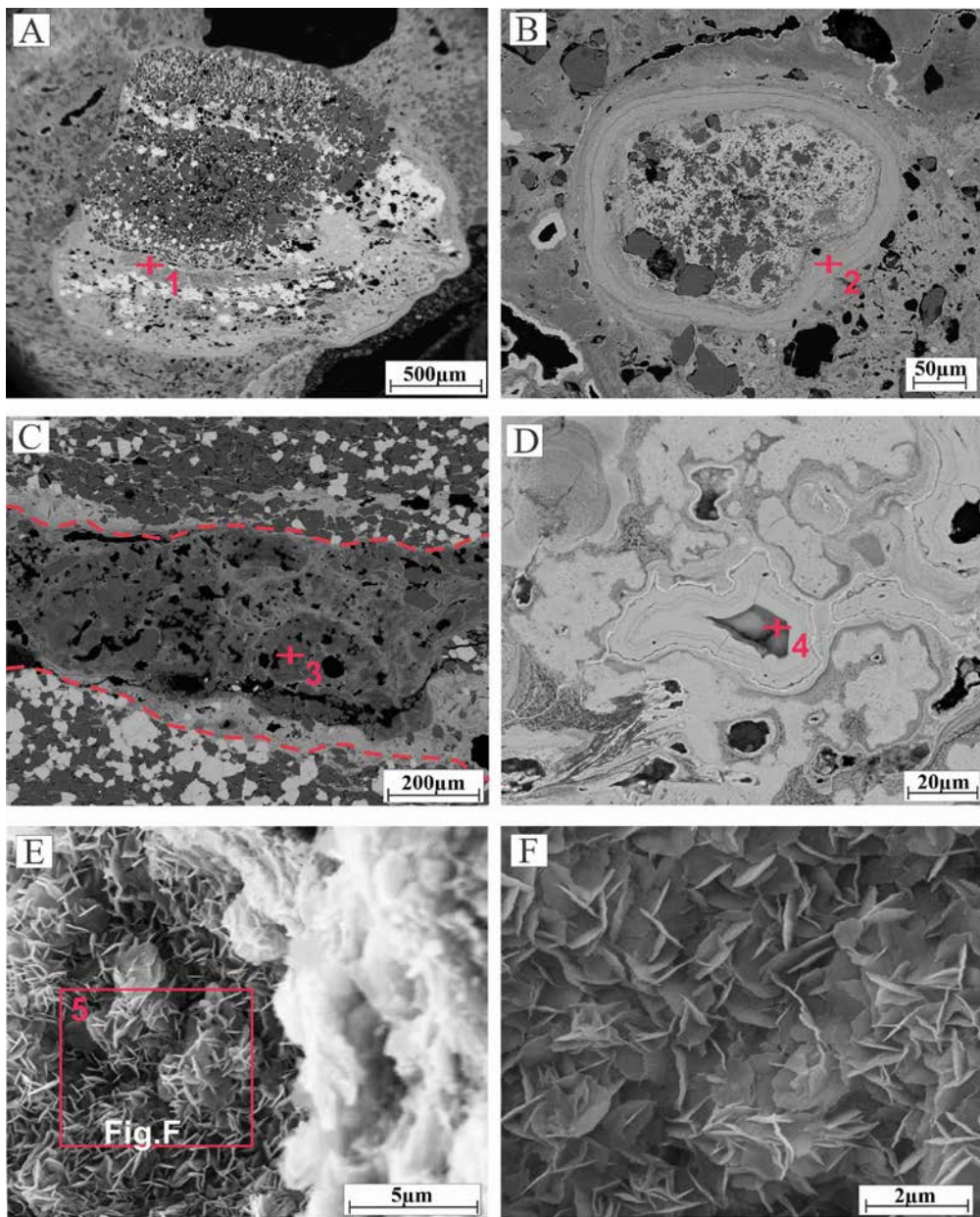


Figure 8. Mesoscopic aspects of crusts with lithorelicts. A) Crust with structural preservation of rhythmic laminations (BIF). B) Crust with milky quartz fragment. Photomicrographs of crusts: C) Alternation between the iron oxide bandings (reddish brown) and microcrystalline quartz, a typical aspect of iron formation; D) Enlarged image of the band corresponding to microcrystalline quartz; E) Contact between iron oxyhydroxide nodule and lateritized BIF fragment; parallel nicols; F) Details of iron oxyhydroxide nodule in previous image; parallel nicols; G) Ferruginous nodules in lateritized BIF; H) Details of lateritized BIF (quartz grains and goethite/hematite mass) inside of goethite nodule; crossed nicols.

Figura 8. Aspectos mesoscópicos das crostas com litorelictos. A) Crosta com preservação estrutural de laminações rítmicas (BIF); B) Crosta com fragmento de quartzo leitoso. Fotomicrografias de crostas: C) Alternância entre bandas de óxido de ferro (marrom avermelhado) e quartzo microcristalino, aspecto típico da formação ferrífera; D) Imagem ampliada da banda correspondente ao quartzo microcristalino; E) Contato entre o nódulo de oxi-hidróxidos de ferro e o fragmento de BIF lateritizado; nicós paralelos; F) Detalhes do nódulo de oxi-hidróxidos de ferro na imagem anterior; nicós paralelos; G) Nódulos ferruginosos de BIF lateritizado; H) Detalhes de BIF lateritizado (grãos de quartzo e massa de goethita / hematita) dentro do nódulo de goethita; nicós cruzados.



1		2		3		4		5	
Element	Concentration								
O	45.431 wt.%	O	40.179 wt.%	O	36.114 wt.%	O	3.688 wt.%	O	0.299 wt.%
Al	14.33 wt.%	Al	4.019 wt.%	Al	17.657 wt.%	Fe	96.312 wt.%	Al	6.945 wt.%
Si	13.968 wt.%	Si	1.82 wt.%	Si	18.675 wt.%		100 wt.%	Si	0.295 wt.%
Fe	26.27 wt.%	Fe	53.9833 wt.%	Fe	27.554 wt.%			Fe	92.461 wt.%
	100 wt.%		100 wt.%		100 wt.%				100 wt.%

Figure 9. Scanning electron microscopy images (SEM) and semiquantitative chemical composition (EDS) of crusts with BIF fragments; A) Fragments of BIFs inside of a ferruginous nodule; B) An iron oxyhydroxide nodule with micro banded ferro-aluminous cortex; C) Lateritized BIF fragment with infilling of iron aluminous material (EDS chemical analysis point 3: kaolinite + goethite); D) Colloform iron oxyhydroxides, typical of Al-poor goethite (EDS chemical analysis point 4); E) Slightly spherical aggregates of platy crystal of Al-bearing goethites (EDS chemical analysis point 5); F) A good detail of the previous crystals habitus.

Figura 9. Imagens de microscopia eletrônica de varredura (MEV) e composição química semiquantitativa (EDS) de crostas com fragmentos de BIF. A) Fragmentos de BIF's dentro de um nódulo ferruginoso; B) Nódulo de oxi-hidróxido de ferro com córtex ferro-aluminoso microbandado; C) Fragmento BIF lateritzado preenchido com material ferroaluminoso (ponto 3 de análise química EDS: caulinita + goethita); D) Aspecto coloforme de oxi-hidróxidos de ferro, típico de goethita pobre em Al (ponto de análise química EDS 4); E) Agregados ligeiramente esféricos de cristais placosos de goethita portadoras de Al (ponto de análise química EDS 5); F) Um bom detalhe do hábito dos cristais anteriores.

3.2 Geochemistry

3.2.1 Chemical Composition and Relationships between the Main Chemical Elements

The chemical compositions of the lateritic crusts in the region of Canaã and Rio Maria investigated here (Table 1) are similar to those of most of the lateritic crusts made up of Fe_2O_3 , SiO_2 and Al_2O_3 , with the first two being much more abundant, with the average values practically identical to each other. Therefore, they are relatively rich in SiO_2 and Fe_2O_3 (Figure 10). The values of Al_2O_3 in turn are comparatively lower than the general lateritic crusts related to bauxite and aluminophosphates. These data, in turn, are consistent with the immature nature of crusts of immature lateritic profiles of Costa (1991) that do not carry bauxite (no aluminum hydroxides). These three components together with loss of ignition (LOI) account for approximately 98% of the total composition of these crusts. TiO_2 contents, in general, are below 1%, which is relatively low for lateritic crusts in general, reflecting parental rocks poor in titanium minerals, such as granitoids and granodiorites. They are also practically devoid of alkaline and alkaline earth elements, which is natural for lateritic crusts. The contents of CaO , MgO and Na_2O are generally approximately or below 0.01%, while those of K_2O can reach a maximum of 0.19%. A very striking aspect of most chemical components, regardless of high or low contents, is their wide variation (Figure 10), so they indicate lateritic crusts with high chemical-mineralogical heterogeneity in terms of the proportions of each of the mineral species, which are few, especially goethite/hematite, quartz and kaolinite. These aspects suggest variable lithological compositions and/or weathering processes and erosion. The contents of P_2O_5 are in 10 samples with values between 0.10 and 0.35% and the other 11 <0.10 in the normality of lateritic crusts, in which the parental rocks do not present phosphorus mineralization.

The samples ITVL 04, ITVL 05, ITVL 15 and ITVL 21 stand out from the others because they have SiO_2 contents relatively low for the

group, from 1.28 to 9.93% and high for Fe_2O_3 (between 61.48 and 96%), and consequently the lowest values of Al_2O_3 and are part of the nodular crust (Figure 10). Most crusts have Al_2O_3 levels that vary from 13.26 to 25%, while only four (ITVL 05, ITVL 15, ITVL 21 and ITVL 36) have lower values (9.8, 0.8, 7.94 and 7.57%, respectively).

The chemical composition presented clearly reflects the domain of a few mineral phases, already presented: hematite, goethite, quartz and kaolinite. Therefore, the contents of Fe_2O_3 for the first two minerals, Al_2O_3 for kaolinite and partly goethite, and SiO_2 mainly for quartz and kaolinite. The LOI values (8.5 to 13.5%) depict the presence of goethite and/or kaolinite, reflecting the presence of kaolinite and goethite. However, in the ITVL 15 sample, this value is 1.1%, practically dominated by hematite, classified as ironstone.

The contents of TiO_2 , equal to or less than 1.0%, are relatively low, suggesting the presence of anatase, as is normal in lateritic crusts. It was not possible to clearly delineate the presence of this mineral in the X-ray diffractograms.

When comparing the average chemical composition (major and minor element oxides) of the lateritic crusts by area investigated, Canaã and Rio Maria (Table 2), there are practically no differences between them. These average values were compared with those of the granitoids of these regions (Table 2) and the dominant rocks, which therefore exerted some strong influence on the formation of these crusts. It is noted that there was practically no increase in the contents of Al_2O_3 , TiO_2 and P_2O_5 ; however, there was a loss of SiO_2 , which is very strong for alkali and alkaline earth alkaline, and absolute gains in Fe and LOI. The same behavior occurs when their values are compared with the crustal average of Rudnick & Gao (2014), with which the granitoids/granodiorites are similar. These relative aspects of gains and losses relative to the crustal average are very evident in Figure 11. It clearly highlights the absolute Fe gains, the loss of SiO_2 and mainly of alkaline and alkaline earth metals, and practically the no variability of Al_2O_3 and TiO_2 . It is noteworthy

that Al_2O_3 , TiO_2 and P_2O_5 present similar patterns, remaining in limbo from immutable to slight gain and loss, a common fact in lateritic formations.

Table 1. Chemical composition of the distinct iron crusts from Canaã and Rio Maria (Major and minor elements in weight percent; trace elements in ppm).

Tabela 1. Composição química das distintas crostas ferruginosas de Canaã e Rio Maria (elementos maiores e menores em porcentagem de peso; elementos traços em ppm).

Samples	Lateritic crusts from Rio Maria					Lateritic crusts from Canaã					
	ITVL-01	ITVL-23	ITVL-25	ITVL-27	ITVL-29	ITVL-34	ITVL-36	ITVL-04	ITVL-05	ITVL-07	ITVL-08
Chemical elements	nodular					Crusts with lithorelicts			nodular		
Wt%											
SiO_2	39.43	35.26	38.09	40.84	26.65	34.73	36.85	9.93	8.78	39.41	46.89
TiO_2	0.59	0.9	1.06	0.42	0.56	0.52	0.29	0.32	0.27	0.64	0.69
Al_2O_3	16.78	17.56	20.49	18.05	19.49	12.64	7.57	11.92	9.8	17.37	10.49
Fe_2O_3	31.48	33.68	27.55	29.27	39.14	42.4	48.51	61.48	65.46	31.15	32.7
MgO	0.02	0.01	0.03	0.09	0.01	0.03	0.03	0.04	0.06	0.02	0.06
CaO	0.03	0.04	0.04	0.01	0.01	0.06	0.07	0.01	0.02	0.02	0.1
Na_2O	0.01	0.01	0.01	0.01	0.01	0.01	0.01	0.01	0.01	0.01	0.01
K_2O	0.05	0.03	0.02	0.22	0.03	0.13	0.12	0.01	0.01	0.05	0.13
P_2O_5	0.07	0.12	0.07	0.06	0.22	0.17	0.15	0.17	0.18	0.11	0.15
LOI	11.2	12.2	12.3	10.7	13.5	9	6.2	12.3	11.3	10.9	8.5
TOTAL	99.66	99.81	99.66	99.67	99.62	99.69	99.8	96.19	95.89	99.68	99.72
ppm											
V	336	353	498	447	851	363	163	147	153	406	214
Cr	875.79	348.95	656.84	492.63	848.42	431.05	246.32	21730.51	22585.77	294.21	88.95
Mn	309.78	232.34	309.78	232.34	154.89	774.5	619.57	387.23	1548.92	77.45	232.34
Co	13.7	4.5	7.1	6	10.3	13.5	29.6	65.9	137.4	6.1	13.6
Ni	16.2	6.1	9.7	6.5	17.7	27.4	48.1	1509.9	1610	8.5	4.8
Cu	168.5	67.5	51.2	21.4	151.2	78.9	49.1	31.3	38.7	446.3	332.6
Zn	11	10	7	10	52	34	41	65	58	3	6
Ga	24.7	22.6	30.6	24.2	32.6	16.3	17.1	14.8	12.6	28.7	19.1
As	9	4	4.6	8.6	20.9	3.1	1.2	n.d.	0.6	4.9	2
Se	0.6	2.3	1.1	0.6	0.7	0.5	0.9	3	1.3	0.7	0.5
Rb	4.2	1.3	1.6	14.8	2.4	4.5	5.7	1.8	1.7	3.8	13.4
Sr	4.7	3.8	3.8	4	2.1	5.3	3.8	1.4	1.7	4.2	6.4
Y	8.8	2.5	3	3.1	5.4	3.4	4.5	4.6	3.3	6.2	25
Zr	532.1	219.6	278.3	609.4	193.3	82.4	51	68.7	38.1	366.3	394.7
Nb	13.5	6.1	7.2	7.5	4.9	4	1.5	3.5	2.3	11.2	11.6
Mo	2.6	2.3	3.3	2.6	8.3	1.9	1.1	0.1	0.1	12.5	3.2
Cd	0.1	0.1	0.1	0.1	0.1	0.1	0.1	0.1	0.1	0.1	0.1
Sn	3	1	1	1	1	1	1	1	1	1	1
Sb	0.1	0.1	0.1	0.3	0.3	1.1	0.4	0.1	0.1	0.1	0.1
Cs	0.1	0.1	0.2	0.9	0.3	0.5	0.7	n.d.	0.1	0.1	0.4
Ba	15	7	9	84	19	110	63	5	80	17	65
Hf	13.4	5.7	7.5	16.4	5.5	2.5	1.3	1.6	1.2	9.6	9.9
Ta	1.3	0.5	0.5	0.8	0.3	0.3	0.1	0.1	0.1	0.9	0.9
W	4	8.3	9.1	8.2	7.8	11.7	14.8	2.6	2.9	6.6	10
Hg	0.06	0.07	0.2	0.17	0.1	0.01	0.02	0.01	0.01	0.03	0.03
Pb	19.4	15.9	13.2	31.8	22	16.5	6.8	17.9	18.3	21	8.5
Bi	0.1	0.1	0.3	0.8	0.5	0.1	0.1	0.1	0.1	0.1	0.1
Th	26.9	6.3	8.1	31.4	13.8	5.6	2.8	3.5	3.5	48.6	13.8
U	9.2	3.2	1.9	7.6	6.3	1.8	1.4	2.1	3.8	17.7	5.6
La	4.5	2.8	1.7	5	3.7	3.4	4.4	6.1	4.2	13.4	9.5
Ce	18.8	4.5	5.7	38.4	18.8	24.9	24.8	14.1	143.4	26.2	23.8
Pr	1.11	0.58	0.42	0.81	1.28	0.9	1.09	1.75	1.2	2.18	2.02
Nd	4.1	1.8	1.6	3	5.8	3.4	4	6.1	4.4	6.7	6.9
Sm	0.85	0.52	0.5	0.61	1.36	0.53	0.98	1.42	0.98	1.02	1.77
Eu	0.26	0.16	0.15	0.18	0.33	0.18	0.27	0.42	0.3	0.23	0.43

ΣLREE	29.62	10.36	10.07	48	31.27	33.31	35.54	29.89	154.5	49.73	44.42
Gd	1.07	0.46	0.45	0.45	1.07	0.72	0.91	1.09	1.26	0.91	2.67
Tb	0.21	0.08	0.08	0.09	0.22	0.11	0.16	0.21	0.17	0.18	0.56
Dy	1.56	0.64	0.56	0.6	1.38	0.63	0.94	1.45	0.89	1.01	4.35
Ho	0.39	0.1	0.12	0.1	0.27	0.15	0.18	0.24	0.19	0.24	0.95
Er	1.32	0.36	0.53	0.46	0.83	0.42	0.65	0.77	0.57	0.74	3.22
Tm	0.21	0.08	0.06	0.08	0.15	0.08	0.12	0.14	0.11	0.14	0.44
Yb	1.74	0.46	0.69	0.75	1.02	0.59	0.7	0.92	0.75	0.96	3.15
Lu	0.3	0.11	0.11	0.15	0.2	0.09	0.1	0.15	0.11	0.19	0.47
ΣHREE	6.8	2.29	2.6	2.68	5.14	2.79	3.76	4.97	4.05	4.37	15.81
ΣREE	36.42	12.65	12.67	50.68	36.41	36.1	39.3	34.86	158.55	54.1	60.23
(La/Sm)_N	3.04	3.8	7.53	3.08	3.13	5.28	3.22	5.42	3.09	1.95	4.7
(La/Yb)_N	1.67	3.94	1.59	4.31	2.35	3.73	4.07	4.29	3.62	9.03	1.95
(Gd/Yb)_N	0.52	0.73	0.8	0.72	0.37	1.56	0.39	0.21	0.85	0.55	0.51
Ce_n/Ce*	1.84	0.76	1.48	3.94	1.93	3.14	2.48	0.96	14.15	1.00	1.17
Eu_N/Eu*	0.84	0.99	0.96	1.01	0.82	0.9	0.87	1	0.83	0.72	0.61

n.d.: not detected.

Table 1. (Continuation).

Lateritic crusts from Canaã											
Samples	ITVL-09	ITVL-12	ITVL-13	ITVL-15	ITVL-20	ITVL-21	ITVL-22	ITVL-02	ITVL-16A	ITVL-16B	
Chemical elements	nodular						massive				
SiO₂	46.5	40.47	51.56	1.28	31.06	4.18	46.01	46.05	38.82	47.05	
TiO₂	1.07	0.59	0.79	0.2	0.41	0.34	0.56	0.72	0.14	0.14	
Al₂O₃	16.55	16.6	13.26	0.8	25	7.94	23.04	20.51	12.87	12.14	
Fe₂O₃	26.88	30.82	23.87	96.19	26.7	70.6	18.06	20.8	33.32	27.1	
MgO	0.02	0.04	0.02	0.01	0.02	0.07	0.01	0.04	0.04	0.07	
CaO	0.04	0.08	0.04	0.02	0.01	0.01	0.01	0.04	0.03	0.1	
Na₂O	0.01	0.01	0.01	0.01	0.01	0.01	0.01	0.01	0.01	0.01	
K₂O	0.05	0.07	0.05	0.01	0.02	0.01	0.07	0.05	0.11	0.19	
P₂O₅	0.07	0.31	0.12	0.1	0.05	0.03	0.03	0.03	0.16	0.18	
LOI	8.5	10.6	9.7	1.1	13.4	10.4	11.9	11.3	12.2	11.5	
TOTAL	99.69	99.59	99.42	99.72	96.68	93.58	99.69	99.55	97.7	98.48	
V	352	493	303	778	139	146	294	320	82	56	
Cr	588.42	595.26	1211.05	88.95	21203.67	41018.39	780	998.95	10139.99	6801.05	
Mn	387.23	154.89	542.12	154.89	697.01	232.34	77.45	1084.24	3872.3	1394.03	
Co	8.2	6.2	7.7	53.2	21.5	67	4.4	26.4	198.2	85.1	
Ni	4.2	8	21.1	183.5	33.1	900.9	4.1	23.5	762.1	498.5	
Cu	68.3	135.6	99.8	247.3	18.1	41	34.3	43.1	29.4	22.7	
Zn	10	24	11	2	12	55	8	4	41	28	
Ga	25.3	28	17.5	73.8	35.8	16.7	43.7	27.3	15.8	12.2	
As	4.9	4.5	2.5	1.3	n.d.	n.d.	3.6	3.6	3.3	2.9	
Se	0.9	1.7	1.2	0.5	2.6	2.9	0.7	0.5	0.5	0.5	
Rb	5.2	10.1	5.6	0.3	2.2	0.8	4.9	3.1	11.8	13.9	
Sr	3.5	10.2	5.6	18.3	2.4	0.5	3	6.7	4.4	36.3	
Y	10.1	3.7	16.9	6.5	2.7	5	2.2	3.7	50.2	27.9	
Zr	328.6	682.7	1449.1	4.5	195.4	117.9	347.4	688.8	135.6	77.7	
Nb	11.8	8.2	6.5	34.2	7	5.2	8.9	6.6	4.8	4.9	
Mo	6.6	5.4	1.9	2.3	0.2	0.7	2.6	1	8.9	5.6	
Cd	0.1	0.1	0.1	0.1	0.1	0.1	0.1	0.1	0.1	0.1	
Sn	1	3	1	11	1	1	1	1	1	1	
Sb	0.1	0.1	0.1	0.1	0.1	0.1	0.1	0.1	0.1	0.1	
Cs	0.1	0.4	0.2	n.d.	n.d.	n.d.	0.1	0.2	0.5	0.7	
Ba	10	37	69	295	69	1	9	30	540	1290	
Hf	10	17.3	51.5	0.1	5.5	3.2	9.8	17	4.8	2.4	
Ta	1.3	0.6	0.4	1.5	0.6	0.4	0.7	0.4	0.7	0.5	
W	19.9	9.1	7.2	9.5	4.2	3.2	15.2	7.4	21.1	1.6	
Hg	0.02	0.01	0.06	0.01	0.09	0.2	0.16	0.21	0.08	0.01	

Pb	20.8	29.3	16.2	6.2	97.5	16.9	16.3	20.1	133.7	69.8
Bi	0.2	0.1	0.1	0.1	0.1	0.1	0.1	0.1	0.4	0.3
Th	15.7	38	24.4	11.9	16.1	9.1	35	8.7	35.4	20.2
U	18.1	3.5	8.6	4.5	4.8	10.1	4.6	1.4	29	18.5
La	1.8	9.3	8.6	20.8	2.9	4.9	5.2	4.5	10.1	5.4
Ce	4.5	214.8	19.6	18.6	74.9	18.3	16.7	20.8	83.4	59.2
Pr	0.35	1.64	1.79	2.32	0.75	1.93	0.96	0.93	2.25	0.98
Nd	1.8	6.5	6	7.3	2.6	8	3.4	3.2	8.2	3.4
Sm	0.33	1.01	1.53	1.61	0.5	1.9	0.55	0.68	2.19	1.06
Eu	0.06	0.24	0.45	0.15	0.16	0.39	0.13	0.17	0.16	0.09
ΣLREE	8.84	233.49	37.97	50.78	81.81	35.42	26.94	30.28	106.3	70.13
Gd	0.66	1.38	1.84	1.5	0.62	1.47	0.32	0.55	3.86	1.86
Tb	0.16	0.15	0.39	0.24	0.09	0.28	0.06	0.09	0.93	0.49
Dy	1.32	0.73	2.75	1.46	0.58	1.8	0.52	0.57	6.94	3.73
Ho	0.32	0.16	0.68	0.31	0.11	0.28	0.13	0.13	1.69	0.98
Er	1.08	0.48	2.52	0.97	0.45	0.91	0.28	0.39	5.38	3.14
Tm	0.22	0.09	0.5	0.15	0.07	0.2	0.05	0.07	0.93	0.49
Yb	1.53	0.75	3.95	1.04	0.63	1.67	1.32	0.64	6.5	3.59
Lu	0.27	0.12	0.79	0.13	0.11	0.24	0.07	0.11	1.02	0.55
ΣHREE	5.56	3.86	13.42	5.8	2.66	6.85	2.75	2.55	27.25	14.83
ΣREE	14.4	237.35	51.39	56.58	84.47	42.27	29.69	32.83	133.55	84.96
(La/Sm)_N	1.56	3.68	2.58	2.46	2.92	2.65	1.48	3.33	7.41	2.46
(La/Yb)_N	0.76	8.02	1.41	12.94	2.98	1.9	2.55	4.55	1.01	0.97
(Gd/Yb)_N	0.89	1.03	1.1	1	0.44	0.5	0.74	0.83	1.22	1.42
Ce_N/Ce*	1.21	11.54	1.07	0.51	11.18	1.32	1.58	2.19	3.79	5.43
Eu_N/Eu*	0.39	0.63	0.83	0.29	0.89	0.69	0.88	0.83	0.17	0.2

Table 2. Average chemical composition for each lateritic crust investigated, as well as for each region (Rio Maria and Canaã) and all together compared with the average of the Upper Continental Crust after Rudnick & Gao (2014), Rio Maria granodiorites after Oliveira *et al.* (2006) and Canaã granitoids after Feio *et al.* (2013).

*Tabela 2. Composição química média para cada tipo de crostas investigadas, para as crostas conforme a sua região (Rio Maria e Canaã e para as duas regiões em conjunto comparadas com a média da Crosta Continental Superior (UCC) de Rudnick & Gao (2014), granodioritos de Rio Maria segundo Oliveira *et al.* (2006) e granitóides de Canaã segundo Feio *et al.* (2013).*

Chemical Elements	Nodular (n=16)	Crusts with lithorelicts (n=2)	Massive (n=3)	Crusts from Rio Maria (n=7)	Crusts from Canaã (n=14)	Lateritic crusts (n=21)	Granodiorites from Rio Maria (n=8)	Granitoids from Canaã (n=16)	UCC
Wt%									
SiO₂	31.65	35.79	43.97	35.98	32.71	33.80	64.1	71.58	66.6
TiO₂	0.59	0.41	0.33	0.62	0.49	0.53	0.42	0.33	0.64
Al₂O₃	15.32	10.11	15.17	16.08	14.16	14.80	14.85	14.12	15.4
Fe₂O₃	40.31	45.46	27.07	36.00	40.37	38.91	2.78	2.58	5.04
MgO	0.03	0.03	0.05	0.03	0.04	0.04	2.29	0.64	2.48
CaO	0.03	0.07	0.06	0.04	0.04	0.04	3.98	2.01	3.59
Na₂O	0.01	0.01	0.01	0.01	0.01	0.01	4.16	4.35	3.27
K₂O	0.05	0.13	0.12	0.09	0.06	0.07	3.23	3.16	2.8
P₂O₅	0.12	0.16	0.12	0.12	0.12	0.12	0.15	0.10	0.15
LOI	10.53	7.60	11.67	10.73	10.26	10.41	1.68	0.93	n.a.
TOTAL	98.64	99.75	98.58	99.70	98.26	98.74	99.3	99.78	-
ppm									
V	369.38	263.00	152.67	430.14	277.36	328.29	n.a.	n.a.	97
Cr	7087.99	338.69	5980.00	557.14	9151.80	6286.91	61	n.a..	92
Mn	358.19	697.04	2116.86	376.17	774.46	641.70	464.67	154.89	774.46
Co	27.05	21.55	103.23	12.10	50.06	37.41	n.a.	n.a.	17.3
Ni	271.52	37.75	428.03	18.81	398.01	271.61	29	n.a.	47
Cu	122.07	64.00	31.73	83.97	113.46	103.63	n.a..	35.37	28
Zn	21.50	37.50	24.33	23.57	23.36	23.43	n.a.	n.a.	67
Ga	28.17	16.70	18.43	24.01	26.52	25.69	20	18.43	17.5

As	5.49	2.15	3.27	7.34	3.10	4.75	n.a.	n.a.	4.8
Se	1.33	0.70	0.50	0.96	1.25	1.15	n.a.	n.a.	0.09
Rb	4.63	5.10	9.60	4.93	5.61	5.39	109	103.37	84
Sr	4.73	4.55	15.80	3.93	7.47	6.29	608	279.58	320
Y	6.81	3.95	27.27	4.39	12.00	9.46	13	16.06	21
Zr	364.13	66.70	300.70	280.87	349.68	326.74	116	211.08	193
Nb	9.35	2.75	5.43	6.39	9.05	8.16	9	10.46	12
Mo	3.42	1.50	5.17	3.16	3.65	3.49	n.a.	n.a.	1.1
Cd	0.10	0.10	0.10	0.10	0.10	0.10	n.a..	n.a..	0.09
Sn	1.88	1.00	1.00	1.29	1.86	1.67	n.a.	n.a.	2.1
Sb	0.13	0.75	0.10	0.34	0.10	0.18	n.a.	n.a..	0.4
Cs	0.25	0.60	0.47	0.40	0.28	0.33	n.a.	n.a.	4.9
Ba	49.44	86.50	620.00	43.86	179.79	134.48	1085	817.01	628
Hf	10.51	1.90	8.07	7.47	10.28	9.34	n.a.	n.a.	5.3
Ta	0.68	0.20	0.53	0.54	0.65	0.61	n.a.	n.a.	0.9
W	7.99	13.25	10.03	9.13	8.61	8.78	n.a.	n.a.	1.9
Hg	0.08	0.02	0.10	0.09	0.07	0.07	n.a.	n.a.	0.05
Pb	23.20	11.65	74.53	17.94	35.18	29.43	n.a.	6.65	17
Bi	0.19	0.10	0.27	0.29	0.14	0.19	n.a.	n.a.	0.16
Th	19.13	4.20	21.43	13.56	20.28	18.04	8	22.62	10.5
U	6.98	1.60	16.30	4.49	9.45	7.80	n.a.	5.07	2.7
La	6.53	3.90	6.67	3.64	7.62	6.30	38.05	45.62	31
Ce	41.32	24.85	54.47	19.41	52.74	41.63	65.73	85.36	63
Pr	1.32	1.00	1.39	0.88	1.50	1.30	6.86	9.31	7.1
Nd	4.75	3.70	4.93	3.39	5.32	4.68	25.68	42.40	27
Sm	1.03	0.76	1.31	0.76	1.18	1.04	4.10	4.95	4.7
Eu	0.25	0.23	0.14	0.22	0.24	0.23	1.15	0.99	1
ΣLREE	55.19	34.43	68.90	28.31	68.61	55.17	141.56	188.62	133.8
Gd	1.08	0.82	2.09	0.73	1.43	1.20	3.03	3.52	4
Tb	0.20	0.14	0.50	0.14	0.29	0.24	0.46	0.52	0.7
Dy	1.35	0.79	3.75	0.90	2.01	1.64	2.04	2.77	3.9
Ho	0.29	0.17	0.93	0.19	0.46	0.37	0.41	0.52	0.83
Er	0.97	0.54	2.97	0.65	1.49	1.21	1.07	1.51	2.3
Tm	0.17	0.10	0.50	0.11	0.26	0.21	0.15	0.23	0.3
Yb	1.33	0.65	3.58	0.85	1.96	1.59	0.94	1.51	1.96
Lu	0.22	0.10	0.56	0.15	0.31	0.26	0.14	0.23	0.31
ΣHREE	5.60	3.28	14.88	3.72	8.20	6.70	8.25	10.80	14.30
ΣREE	60.80	37.70	83.78	32.03	76.80	61.88	149.81	199.42	148.10
(La/Sm)_N	3.32	4.25	4.40	4.15	3.26	3.56	5.90	6.48	-
(La/Yb)_N	3.96	3.90	2.18	3.09	4.00	3.70	28.02	41.49	-
(Gd/Yb)_N	0.69	0.98	1.16	0.73	0.81	0.78	2.74	2.53	-
Ce_N/Ce*	3.48	2.81	3.80	2.22	4.08	3.46	0.88	0.88	-
Eu_N/Eu*	0.77	0.89	0.40	0.91	0.64	0.73	1.42	0.95	-

The correlations SiO₂ vs. Fe₂O₃ and Al₂O₃ vs. Fe₂O₃ (Figure 12A and B) classically negative and in part TiO₂ vs. Fe₂O₃ (Figure 12C) characterize the lateritic nature of these crusts, also provided by the positive TiO₂ vs. Al₂O₃ (Figure 12D). They demonstrated that the crusts constitute a probable absolute supply of Fe, and loss of SiO₂ or, they reflect

parent rocks with strong contrasts in the chemical contents of these elements, as already demonstrated. This was reinforced by Al₂O₃ and TiO₂, which have large ranges in contents. The very low contents of TiO₂ (ITVL-15, ITVL-16A, ITVL-16B, ITVL-21) and Al₂O₃ suggest an ultramafic parent rock.

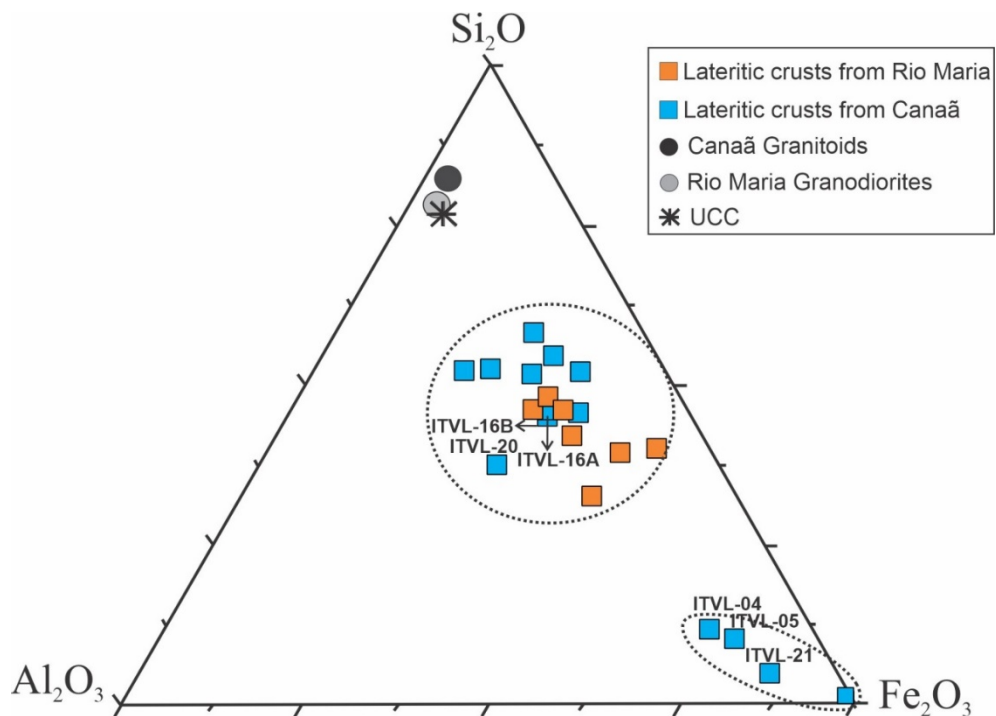


Figure 10. Diagram of Al_2O_3 - SiO_2 - Fe_2O_3 showing the distribution of the chemical composition of crust samples from the Domains Rio Maria and Canaã compared with the average of the UCC after Rudnick & Gao (2014), Rio Maria granodiorites after Oliveira *et al.* (2006) and Canaã granitoids after Feio *et al.* (2013). The sample ITVL-15 plots in the Fe_2O_3 vertex.

*Figura 10. Diagrama Al_2O_3 - SiO_2 - Fe_2O_3 mostrando a distribuição da composição química das amostras das crostas dos Domínios Rio Maria e Canaã, em comparação com a média UCC de Rudnick & Gao (2014), granodioritos de Rio Maria segundo Oliveira *et al.* (2006) e granitóides de Canaã segundo Feio *et al.* (2013). A amostra ITVL-15 plota no vértice do Fe_2O_3 .*

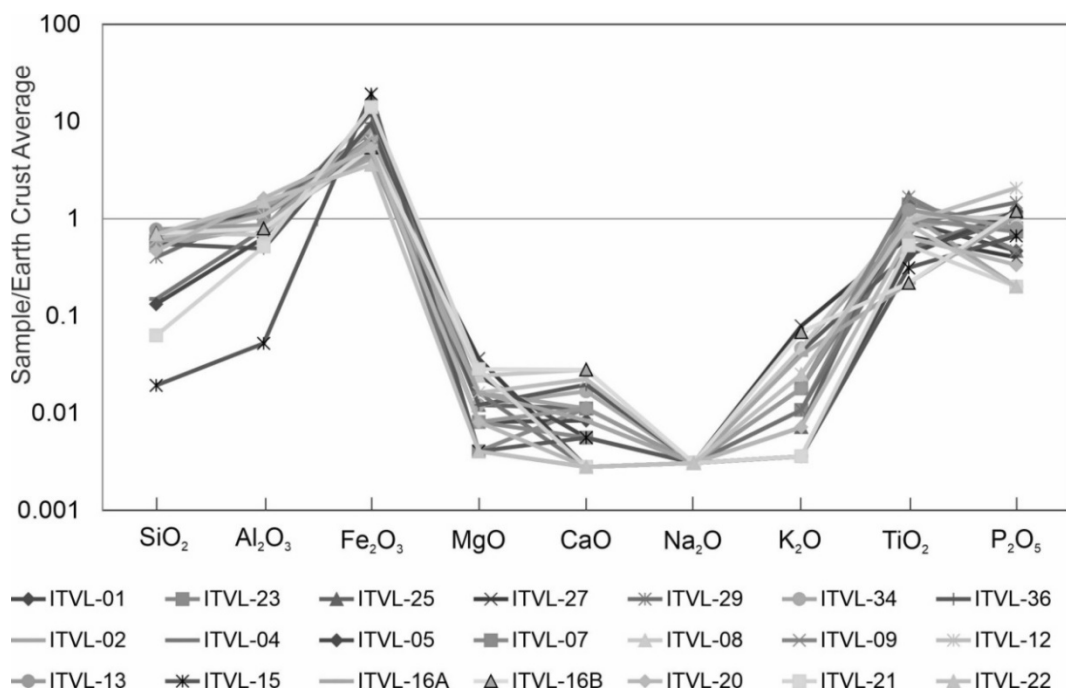


Figure 11. Distribution pattern of major chemical elements normalized to the Earth upper crustal average of Rudnick & Gao (2014) in samples of lateritic crusts.

Figura 11. Padrão de distribuição das concentrações dos principais elementos químicos nas crostas lateríticas normalizadas a média da crosta superior da Terra segundo Rudnick & Gao (2014).

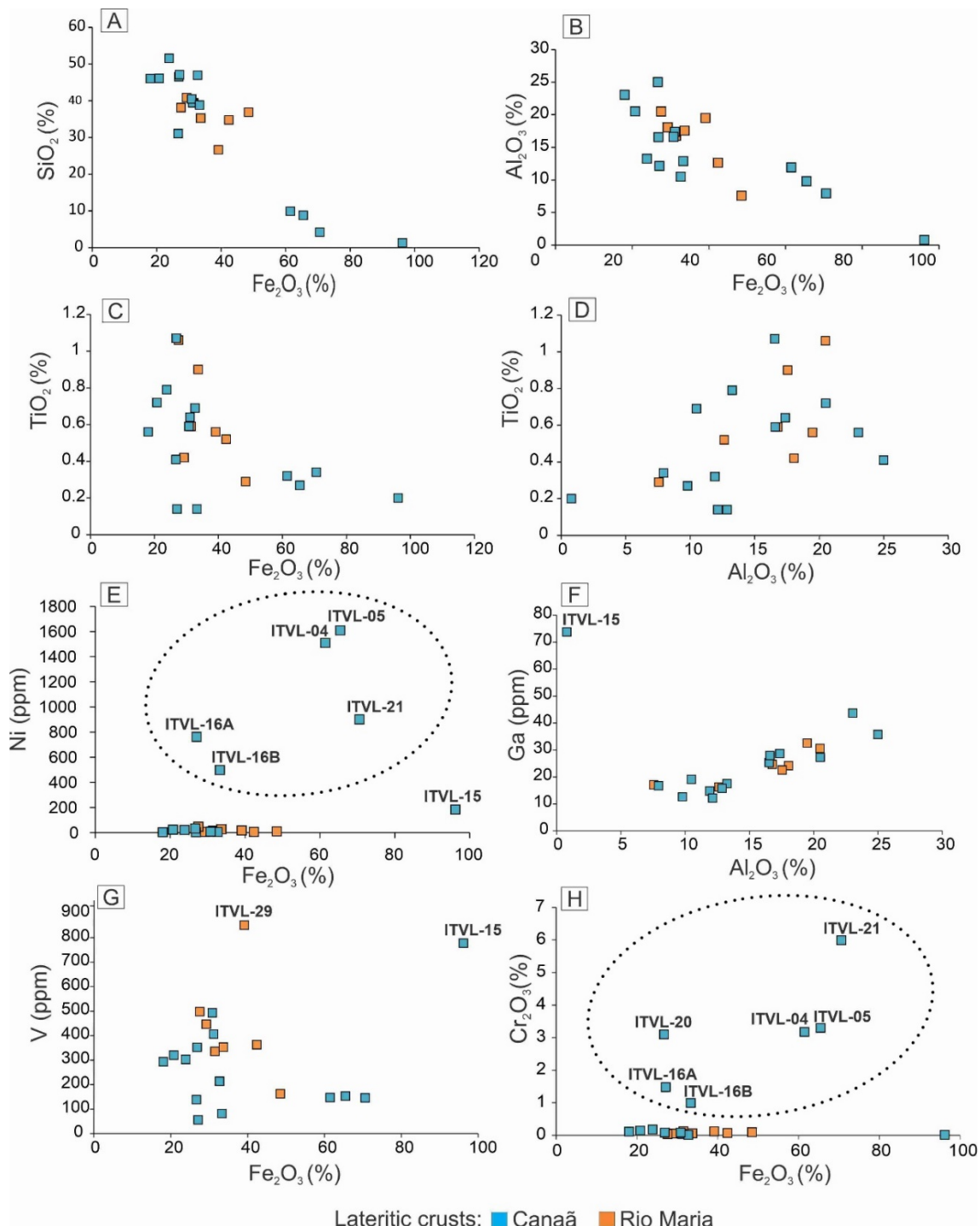


Figure 12. Chemical dispersion diagrams for lateritic crusts investigated in Canaã and Rio Maria. The dotted circle in E and H indicates the potential samples derived from ultramafic rocks after their contents in Ni, Cr and Fe_2O_3 .

Figura 12. Diagramas de dispersão química para crostas lateríticas investigadas em Canaã e Rio Maria. O círculo pontilhado nas figuras E e H indica as amostras com potencial derivação de rochas ultramáficas com base nos teores de Ni, Cr e Fe_2O_3 .

3.2.2 Concentration and Behavior of the Trace Elements

The average concentrations of trace elements of the studied lateritic crusts (Tables 1 and 2; Figures 12 and 13) when compared to those of the upper continental crust (UCC) average are:

- below to it for Mn, Zn, Rb, Sr, Y, Nb, Sn, Cs, Ba and Ta; and;
- above for V, Cr, Co, (Ni), Ga, As, Se, Zr, Mo, Hf, W, Hg, Pb, Bi, Th and U.

This pattern was also partially observed when compared with the granitoids of the region, in which data are available for few trace elements and basically only for the granites of Canaã. It is worth mentioning that in the set, the values of the concentrations of the trace elements are very variable, similar to those of the major elements, so in each set (below or above the UCC), it contains isolated trace elements, whose contents may be above and below or even comparable to those of the UCC. This is well depicted in Figure 13. Among those elements classified as those always below the UCC, Zn, Rb, Sr and Cs stand out. Only Ba and Nb in the two samples exceed the crustal average. It should be noted that barite was identified locally on a micrometric scale (Figure 4E). On the other hand, in the group above the UCC, the variations are wide, going from far below and well above the UCC, being more striking for V, Cr, Mn, Ni, Cu, As, Zr, Mo and Hf. The values of Se, V and W are always above (Figure 13). Among these striking V, Cr and Ni are at the level of geochemical

anomalies, especially Cr. The elements Cr and Ni are strong geochemical signatures for ultramafic rocks. The contents of Cr reach 41,018 ppm in ITVL 21, which corresponds to approximately 4.10% Cr. With this content, the presence of the most characteristic mineral of Cr, chromite, was expected, considering the ultramafic environment already inferred during geological mapping in the field in small outcrops, represented by talc schists and serpentinites. Chromite was identified by XRD in sample ITVL 21 (Figure 3D). Therefore, several samples (ITVLs 4, 5, 16A, 16B, 20 and 21) with anomalous values, not only Cr but also Ni, cannot have been derived from granitoids dominant in the study region but also from ultramafic rocks, for which these anomalies are typical and unique. Ultramafic rocks mineralized in these elements are already known around the region, such as the nickel deposit of Vermelho, with the development of complete lateritic profiles (Oliveira *et al.*, 1992) and occurring around the world (Schellmann, 1986; 1994).

The positive geochemical correlations Al_2O_3 vs. Ga (Figure 12F) and the slightly positive trends V and Cr with Fe_2O_3 (Figure 12G and H) reinforce the classic lateritic nature of these crusts (Hieronymus *et al.*, 2001). In the specific case of Cr and Ni, they distinguish the crusts probably derived from granitoids from those of ultramafic rocks (Figure 12G and H, dotted circle). Relegating the two outlier samples (ITVL-15 and ITVL-29) in the diagram of Figure 12G, the correlation V vs. Fe_2O_3 shows a negative trend.

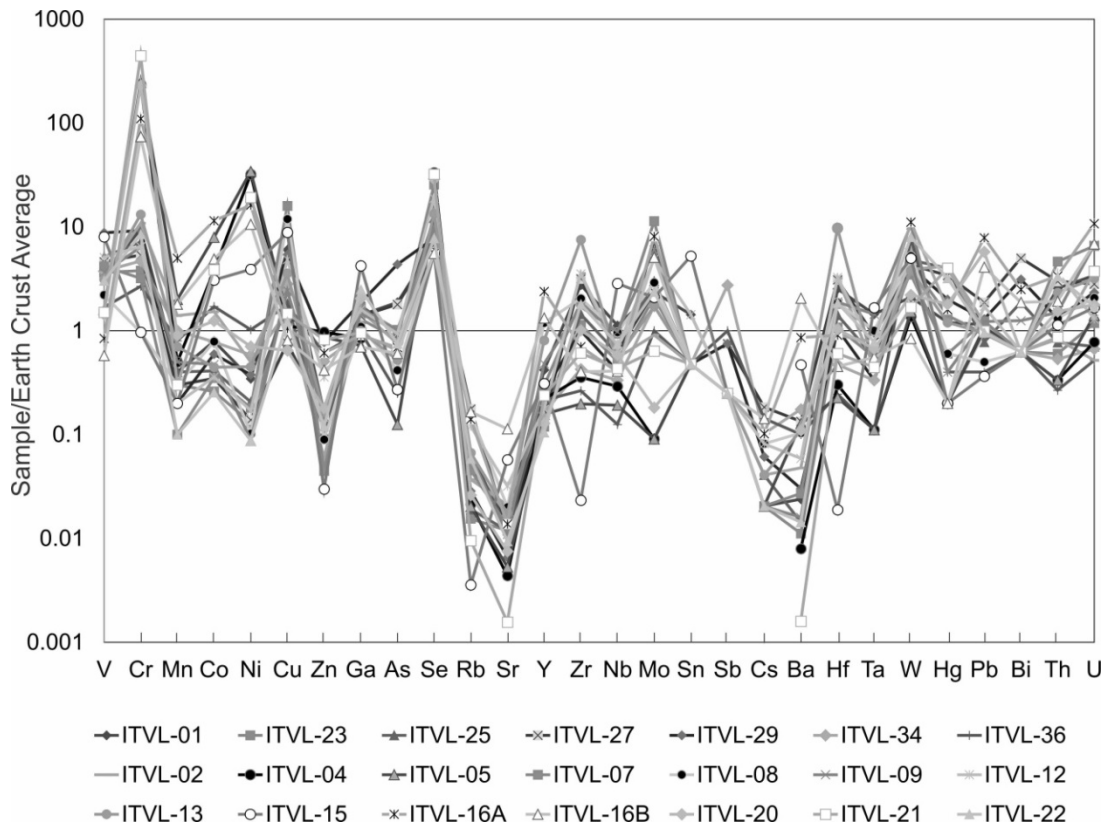


Figure 13. Distribution pattern of the contents of chemical trace elements normalized to the Earth upper crustal average (UCC in Table 2) of Rudnick & Gao (2014) for the studied lateritic crusts.

Figura 13. Padrão de distribuição das concentrações dos elementos traços nas crostas lateríticas investigadas e normalizadas para a média da crosta superior da Terra (UCC na Tabela 2) de Rudnick & Gao, (2014).

Considering the cluster analyses, the data allow us to identify the major geochemical associations and discriminate some crusts after geological affinities (Figure 14). Three general geochemical associations were identified (Figure 14A): $\text{SiO}_2\text{-Al}_2\text{O}_3\text{-Fe}_2\text{O}_3\text{-TiO}_2$ -PF as LOI-K₂O-Mn-Ba-Sr-Zr-Hf-Cr-Ni-Co-..., which represents the major chemical components and, as a consequence, the lateritic crust forming minerals (goethite/hematite, kaolinite and quartz; anatase?) and related trace elements; it detaches Cr-Ni, a signature for ultramafic parent rock; the association $\text{P}_2\text{O}_5\text{-Mo-Th-W-Cu-LREE-As-V-Ga-Nb-Ta-Sn-Sb}$ with emphasis on P and LREE; and Y-HREE-(U), showing the deep fractionation of REEs into LREEs and HREEs. The treatment also discriminates three crust groups (Figure 14B): a) possible ultramafic-derived crusts (samples ITVL 16, 16A, 04, 05, 20 and 21 with high contents of Cr and Ni); b) granitoid/granodiorite-derived crusts (the other samples, except for ITVL 15);

c) the “crust” sample ITVL 15, an ironstone with 96.19% Fe_2O_3 . This sample is from mineralogy and chemistry completely distinct from other samples. Chemical data and geochemical associations have been shown to be effective in discriminating lateritic crusts and together with the concentration and mineralogy to discriminate potential parent rocks.

The TiO_2 vs. Zr dispersion diagram (after Hallberg, 1984) for the studied samples allowed one to interpret the probable petrological natures of the parental rocks of these lateritic crusts (Figure 15). Most are established in the field of andesites and dacites, volcanic correspondents for the TTGs of Canaã-Rio Maria, here generically called granitoids/granodiorites. Crust samples that showed geochemical signatures of derivation from ultramafic rocks plot on the basalt limb (Figure 15, dotted red circle), where the diagram does not predict a specific field.

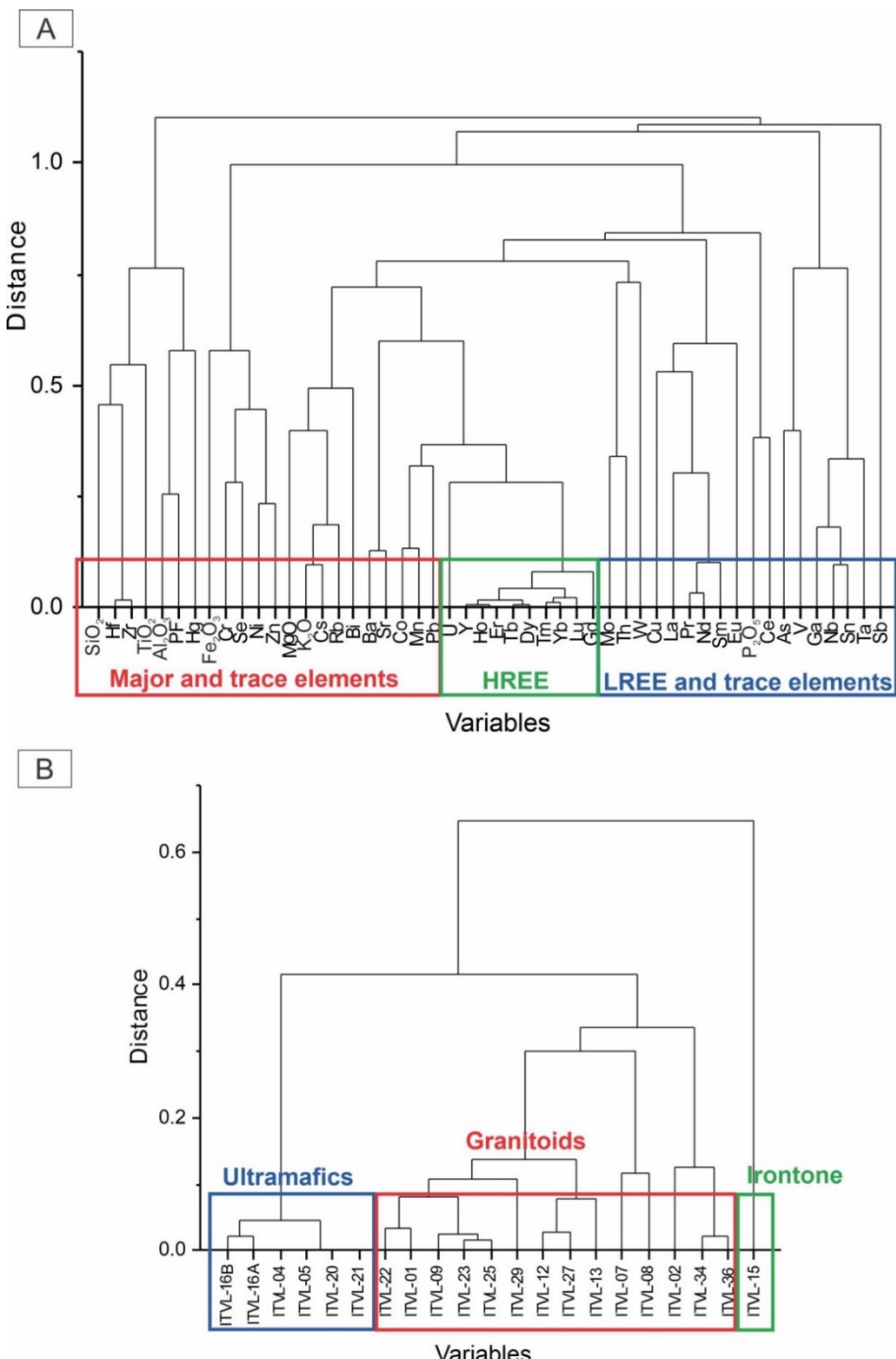


Figure 14. Dendrograms after chemical analysis. A) It is possible to identify up to three possible chemical associations: SiO₂-Al₂O₃-Fe₂O₃-TiO₂- (PF as LOI)-K₂O-Mn-Ba-Sr-Zr-Hf-Cr-Ni-Co-...; P₂O₅-Mo-Th-W-Cu-LREE-As-V-Ga-Nb-Ta-Sn-Sb; and Y-HREE-(U); B) The analyzed crust samples discriminate three groups: a) possible ultramafic derived crusts (ITVL 16, 16A, 04, 05, 20 and 21); b) granitoid/granodiorite derived crusts (the others, with the exception of ITVL 15); and c) the “crust” sample ITVL 15, an ironstone with 96.19% Fe₂O₃.

Figura 14. Dendrogramas segundo os dados das análises químicas. A) É possível identificar até três associações químicas: SiO₂-Al₂O₃-Fe₂O₃-TiO₂- (PF as LOI)-K₂O-Mn-Ba-Sr-Zr-Hf-Cr-Ni-Co-...; P₂O₅-Mo-Th-W-Cu-LREE-As-V-Ga-Nb-Ta-Sn-Sb; e Y-HREE- (U); B) As amostras das crostas analisadas discriminam três grupos: a) possíveis crostas derivadas de rochas ultramáficas (ITVL 16, 16A, 04, 05, 20 e 21); b) crostas derivadas de granitóides / granodioritos (as demais, exceto ITVL 15) e c) a amostra de “crosta” ITVL 15, um ironstone com 96,19% de Fe₂O₃.

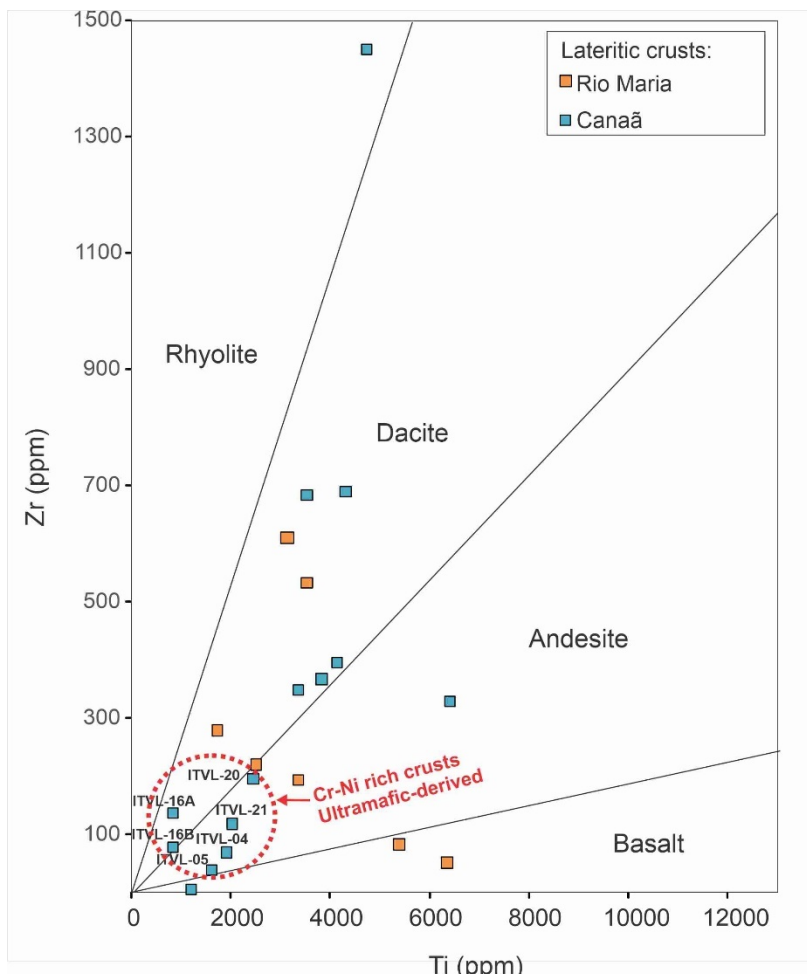


Figure 15. Samples of Canaã and Rio Maria lateritic crusts plotted on a Ti vs. Zr dispersion diagram to identify the probable nature of parental rocks for these crusts. Elaborated according to the diagram of Hallberg (1984). The dotted red circle probably indicates the lateritic crusts derived from ultramafic rocks.

Figura 15. Amostras das crostas lateríticas de Canaã e Rio Maria plotadas no diagrama de dispersão Ti vs. Zr para identificar a provável natureza das rochas parentais dessas crostas. Elaborado de acordo com o diagrama de Hallberg (1984). O círculo vermelho pontilhado indica as amostras de crostas lateríticas, derivadas possivelmente de rochas ultramáficas.

The correlation Zr vs. Hf (Figure 16A) is practically linearly positive, suggesting the presence of the mineral zircon (demonstrated by the strong positive correlation Zr vs. SiO₂) as a carrier of these elements, but the Zr/Hf ratios varying between 28 and 40 indicate rocky sources with variable chemistry, represented by the broad spectrum of granitoids (TTGs) in the region. The correlation Nb vs. Ta is also positive (Figure 16B), and these elements do not correlate Zr and Hf, as is common, suggesting that they must constitute their own mineral or are housed in other minerals. Except for the elements

mentioned, Zr concentrations do not show a significant correlation with the other chemical elements, not even with REE and TiO₂, generally observed in lateritic profiles (Costa *et al.*, 2014; 2016). The correlations showed a tendency toward a negative trend (Figure 16C to F), which is not common to laterites.

However, U and Th showed a significant positive correlation in these crusts (Figure 16G), a geochemical characteristic of lateritic crusts in general, in which Th has a strong relationship with Fe hydroxides (Shuster *et al.*, 2005).

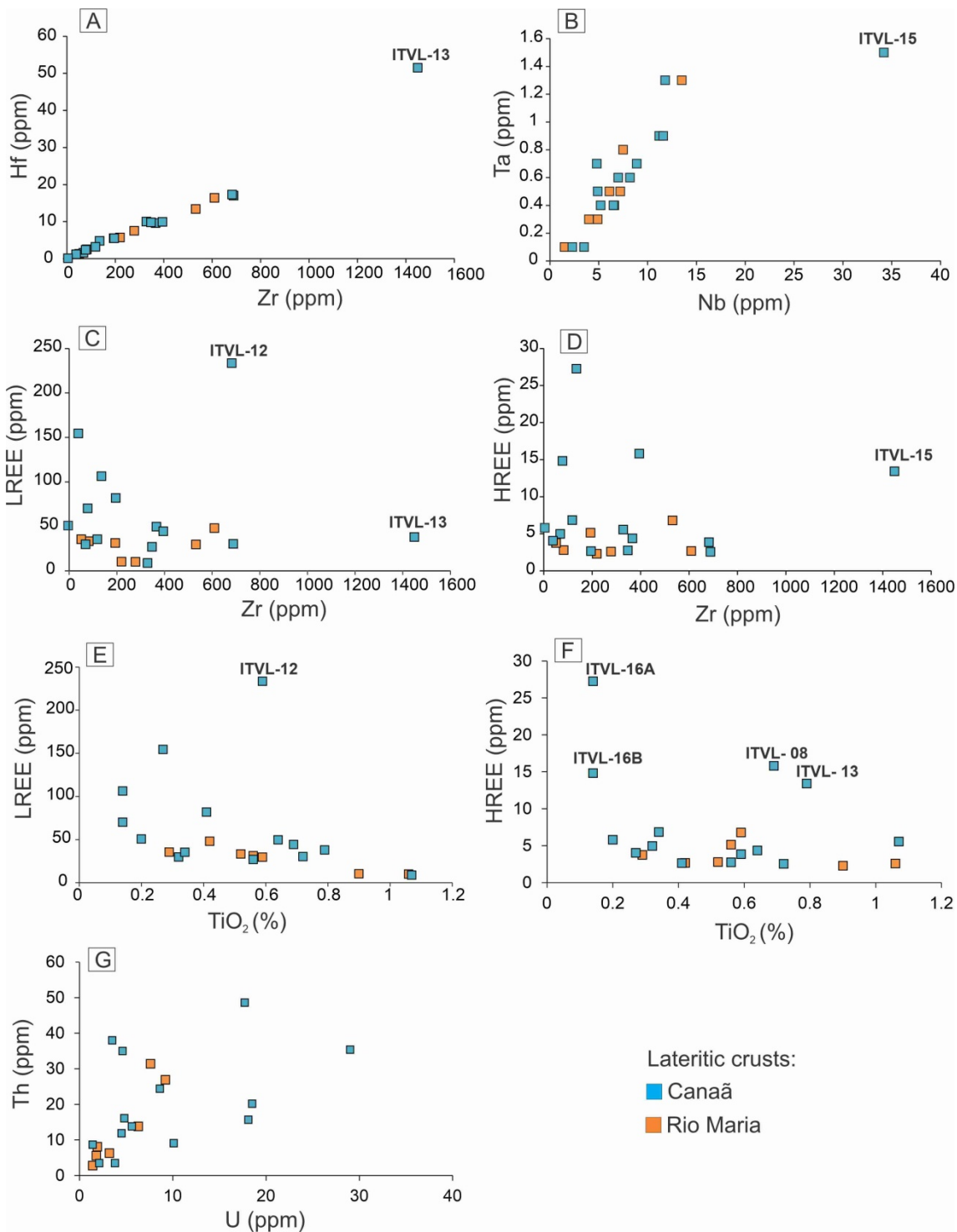


Figure 16. Chemical dispersion diagrams with emphasis on trace elements for lateritic crusts investigated in Canaã and Rio Maria.

Figura 16. Diagramas de dispersão química com ênfase aos elementos traços para as crostas lateríticas investigadas em Canaã e Rio Maria.

3.2.3 Concentrations and Geochemical Behavior of Rare Earth Elements

The concentrations of rare earth elements (REE) in the investigated crusts

(Table 1) are indistinctly both in their average values, as well as individually, below the crustal average and in most of the region's granitoids, except for Ce, which reaches 143 and 214 ppm in the ITVL 5 and ITVL 12

samples, respectively. The ITVL 23 sample displays the lowest total concentration (12.65 ppm for Σ REE), and ITVL 12 displays the highest (237.35 ppm Σ REE).

On the other hand, the correlation is strongly positive between HREE and Y and between Y and Ba (not indicated in Figure 16). The Y contents range from 2.2 to 50.2, which are predominantly below the crustal average. It is likely that REEs and Ba constitute their own minerals or are housed in a specific mineral, other than zircon.

The fractionation between LREEs and HREEs (Tables 1 and 2) measured by the ratio (La/Yb)N shows impoverishment in HREE, which was lower in sample ITVL 09 (0.76) and higher in ITVL 15 (12.94). Among the LREEs, the fractionation measured by the ratio (La/Sm)N varied from 1.48 to 7.53, therefore being more accentuated than in the HREE, according to the ratio (Gd/Yb)N, which varied between 0.21 and 1.42.

Most of the crust samples showed positive Ce anomalies (Ce^*_N/Ce^*), reaching 14.15 (Table 1) (Figure 17A and B), which were more elevated in samples ITVL 05, ITVL 12, ITVL 20 and ITVL 16B (11.81, 14.15 and 5.43, respectively), with geochemical ultramafic inheritances, except for ITVL 12. Positive Ce anomalies are frequently observed in lateritic environments and occur when Ce^{+3} oxidizes to Ce^{+4} , which precipitates in general as cerianite (Braun *et al.*, 1990; Oliveira & Imbernon 1998, Costa *et al.*, 2014). These same crusts show, in part, a slight negative Eu anomaly (Eu^*_N/Eu^*) (Figure 17B and C), which varies between 0.61 and 1.003. It is not common, but it is observed in clay minerals in weathering profiles, according to Li and Zhou *et al.* (2020), when Eu^{+3} is reduced to Eu^{+2} . Chondrite-normalized patterns after Taylor & McLennan (2001) values depict europium anomalies in samples ITVL 09, ITVL 15, ITVL 16B and ITVL 16A (Figure 17B and C). Two samples (ITVL-04 and ITVL-07; Figure 17 C and D) do not display any Ce or Eu anomalies. In general, the distribution pattern of REE normalized to chondrites enhances its lateritic nature.

3.3 Evolution of the Immature Lateritic Landscape

The investigated lateritic crusts, located in the lowland areas around the Carajás Range or plateaus, are nodular, massive and with lithorelicts, and they have mineralogical and geochemical characteristics equivalent to immature laterites. They are relatively younger than the mature laterites that make up the upper land of Carajás. In the specific case, derived from granitoid and partly ultramafic rocks, according to textural and geochemical signatures. It is likely that the region studied has already been covered equally by mature laterites that have shaped the Carajás upper land since the Paleogene until the Miocene or Pleistocene (Costa, 1991; 1997; Costa & Araújo, 1997; Costa *et al.*, 1997; Monteiro *et al.*, 2018; Silva & Costa, 2020; Negrão & Costa, 2021), which were largely removed by erosive denudation events. The erosive debris is currently resting in deep valleys and forms thick debris cover inside the Carajás Range and plateaus in part similar, only to a lesser extent, to Pilbara in Australia (Ramanaidou & Morris, 2003; Morris & Ramanaidou, 2007).

In the study area, almost everything was removed, probably through remounting erosion (Monteiro *et al.*, 2018), leading to an unevenness of more than 300 m, with some testimony hills, and therefore, much exposure of primary rocks and their saprolites. This denudation activity must have occurred during the Middle Miocene, corresponding to the Itacaiúnas Surface under the age of 10 Ma (Monteiro *et al.*, 2018), which extends through Canaã and Rio Maria. For this to have happened, the climate must have been hot and dry, with savanna vegetation. In the Upper Miocene, a new immature lateritic weathering phase was established, meaning a hot and humid tropical climate and forest cover, which was consolidated during the Pliocene, when the climate returned to dry and with restricted vegetation cover, similar to the one concluded by Costa *et al.* (2021 submitted) in the Rondon do Pará region, west of the study area.

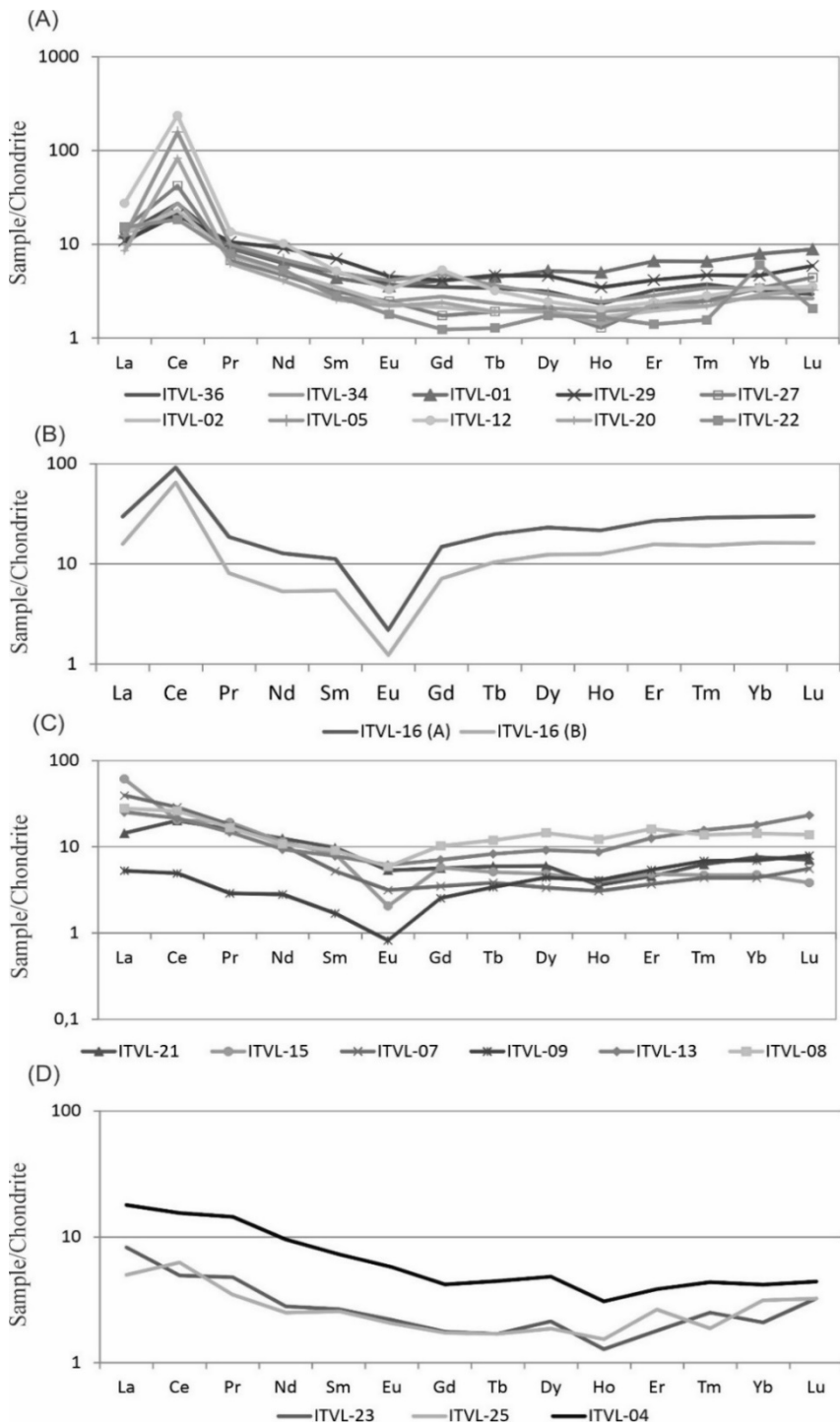


Figure 17. Distribution pattern of REEs normalized to Taylor & McLennan (2001) chondrites in samples of lateritic crusts. A) Samples that show very expressive positive Ce anomalies; B) Only two samples mineralized in Cr, showing both positive Ce and negative Eu anomalies; C) Six samples from nodular lateritic crusts (one mineralized in Cr) exhibiting negative Eu anomalies; D) Three samples from nodular crusts (one mineralized in Cr), without Eu anomalies, although subtle negative or positive Ce anomalies can be inferred in two samples.

Figura 17. Padrão de distribuição das concentrações dos ETR das crostas lateríticas investigadas normalizadas aos condritos de Taylor & McLennan (2001). A) Amostras que mostram anomalia positiva muito expressiva de Ce; B) Duas amostras mineralizadas em Cr, apresentando anomalias de Ce positiva e Eu negativa; C) Seis amostras, todas nodulares, apenas uma mineralizada em Cr, exibindo somente anomalia negativa de Eu; D) Três amostras de crostas nodulares, apenas uma mineralizada em Cr, sem anomalias de Eu, embora se possa inferir sutil anomalia negativa ou positiva de Ce em duas delas.

During the Pleistocene (Häggi *et al.*, 2017; Allard *et al.*, 2018; Zular *et al.*, 2019; Mathian *et al.*, 2020), as in Carajás, and several other parts of the Amazon region, it experienced a new hot and humid phase, which remains to the present, leading to biochemical and physical degradation of the profiles, especially their crusts, as they are the outcropping part of them, and as a consequence gave rise to Oxisols and Argisols (Nahon *et al.*, 1989; Horbe & Costa, 2005), which are the most abundant materials on the surface today, including the exposure of rock blocks, which have increased in recent times as a consequence of rainforest removal by human activities.

4 Conclusions

The ferruginous crusts investigated in the Canaã - Rio Maria geological region mainly occur in isolated blocks resting close to the outcropping of granitoids (TTG). Textural features suggest formation *in situ* with strong physical-chemical degradation. The mineralogical composition dominated by goethite, hematite, partly kaolinite and much quartz reinforce nature as immature crusts, reinforced by their field occurrence, strengthened by microtextural aspects. They are mainly nodular and massive; however, they partly comprise fragments of BIF and quartz veins and are therefore inherited. The chemical composition is dominated by SiO₂, Fe₂O₃ and Al₂O₃ and LOI, which make up 98% of the rock. Their contents, however, are very variable, in fact portraying very heterogeneous crusts, of course suggesting distinct parent rocks. The lateritic nature of these crusts is further confirmed in addition to mineralogy and textures by the negative correlations SiO₂ - Fe₂O₃, SiO₂-Al₂O₃, Al₂O₃-Ga, TiO₂-Al₂O₃ and many others related to trace elements and rare earth elements. Additionally, their contents and geochemical associations (major and trace elements) and mineralogy well discriminate lateritic crusts derived from granitoids and ultramafic rocks. Those ultramafic-derived samples were mainly broken down by anomalous Cr (including chromite presence) and Ni values. Therefore, the studied region has potential for

Cr and Ni mineralization, in which the second is already known in the surrounding region in Vermelho.

It is likely that the Canaã-Rio Maria region, bordering the Serra dos Carajás, was already covered by mature laterites, which were completely removed by erosive events during the Middle Miocene under dry conditions. In the Upper Miocene and Pliocene under a tropical climate and then dry in the area already lowered, immature profiles were established, to which the studied crusts belong as part of the Itacaiúnas Geomorphic Surface. In the Pleistocene, under a hot and humid climate until today, they were partially degraded with the formation of Oxisols and Argisols.

Acknowledgments. To ITV-Belém for financial support through the Paleoclima project; CNPQ through the GEOCIAM project (Process: 573733/2008-2); Grant and Research Project to the first author (Processes: 305015/2016-8, 304.519/2009-0, and 442871/2018-0); Scientific Initiation Scholarship to the second and third author; likewise, Grant to fourth author. We also thank Prof. Dr. Arnaldo Queiroz (UFPA), Profa. Dra. Gilmara Feio (UNIFESPA), and Dr. Tasso Guimarães (ITV) for their participation during fieldwork.

Referências

- Allard, T., Gautheron, C., Riffel, S.B., Balan, E., Soares, B.F., Pinna-Jamme, R., Derycke, A., Morin, G., Bueno, G.T. & do Nascimento, N. 2018. Combined dating of goethites and kaolinites from ferruginous duricrusts. Deciphering the Late Neogene erosion history of Central Amazonia. *Chem. Geol.*, 479: 136-150.
- Araújo, O.J.B., Maia R.G.N, João M.X.S.J. 1991. Aspectos gerais. *In: Araújo O.J.B. & Maia R.G.N. (eds.). Programa Levantamentos Geológicos Básicos do Brasil. Programa Grande Carajás. Serra dos Carajás. Folha SB.22-Z-A. Estado do Pará. Brasília: DNPM-CPRM*, p. 3-10.
- Bignelli, P.A., Paradella W.R., Morais M.C. & Sant'Anna M.V. 1998. Avaliação da potencialidade de discriminação de subunidades litológicas do Complexo

- Xingu na região de Salobo, Província Mineral de Carajás, Brasil; através de imagens de radar de abertura sintética. In: 9º Simpósio Brasileiro de Sensoriamento Remoto, Santos, Brasil. Anais... Santos, INPE, p. 371-381.
- Braun, J.J., Pagel M., Muller J.P., Bilong P. Michard A. & Guillet B. 1990. Cerium anomalies in lateritic profiles. *Geochemica et Cosmochimica Acta*, 54(3): 781-795.
- Coelho, M.R., Santos H.G., Silva E.F. & Aglio M.L.D. 2002. O recurso natural solo. In: Manzatto C.V., Freitas Jr. E.F, Peres J.R.R. (eds.). *Uso agrícola de solos brasileiros*. Rio de Janeiro, Embrapa solos, p. 1-11.
- Costa, M.L. 1991. Aspectos geológicos dos lateritos da Amazônia. *Revista Brasileira de Geociências*, 21 (2): 146-160.
- Costa, M.L. 1997. Lateritisation as a major process of ore deposit formation in the Amazon region. *Exploration and Mining Geology, London*, 6 (1): 79-104.
- Costa, M.L. 2007. Introdução ao intemperismo laterítico e à lateritização. In: Licht, O.A.B., Silva, C.R.S., Bandeira de Melo C.S. (eds.). *Prospecção geoquímica*. Rio de Janeiro, Sociedade Brasileira de Geoquímica, p. 299-344.
- Costa M.L. & Araújo E.S. 1997. Caracterização mineralógica e geoquímica multi-elementar de crostas ferruginosas lateríticas tipo minérios de ferro em Carajás. São Paulo. Geociências, 16(1):55-86.
- Costa, M.L., Lemos, V.P., Villas, R.N. 1997. The Bauxite of Carajás Mineral Province. In: Carvalho, A., Melfi, A.J., Lucas, Y. (eds.). *Brazilian Bauxites*. USP/FADESP/ORSTOM, São Paulo/Paris, pp. 137-159.
- Costa, M.L., Cruz, G.S., Almeida, H.D.F. & Pöllmann, H. 2014. On the geology, mineralogy and geochemistry of the bauxite-bearing regolith in the lower Amazon basin: Evidence of genetic relationships. *Journal of Geochemical Exploration*, 146: 58-74.
- Costa, M.L., da Leite, A.S. & Pöllmann, H. 2016. A laterite-hosted APS deposit in the Amazon region, Brazil: the physical-chemical regime and environment of formation. *J. Geochem. Explor.*, 170: 107-124.
- Costa, M.L., Abreu, D.S., Santos, P.H.C. & Leite, A.S. 2021. An Immature Lateritic Iron Crust and its Topsoil in Amazon: Mineralogical and Geochemical Evolution Supporting Paleoclimatic Changes During the Neogene. *Journal of South American Earth Science* (submitted).
- Dall'Agnol R., Oliveira M.A., Almeida J.A.C., Althoff, F.J., Leite, A.A.S., Oliveira D.C. & Barros C.E.M. 2006. Archean and paleoproterozoic granitoids of the Canaã metallogenic province, Eastern Amazonian craton, Brazil. In: Symposium on Magmatism, crustal evolution, and metallogenesis of the Amazonian Craton. *Abstracts Volume and Field Trips Guide*. Belém, PRONEX-UFPB/SBG-NO, p. 99-150.
- Dall'agnol R., Oliveira D.C., Guimarães F.V., Gabriel E.O., Feio G.R.L., Lamarão C.N., Althoff F.J., Santos, P.A., Teixeira M.F.B., Silva A.C., Rodrigues D.S., Santos M.J.P., Silva C.R.P., Santos R.D. & Santos P.J.L. 2013. Geologia do Subdomínio de Transição do Domínio Carajás – Implicações para a evolução arqueana da Província Carajás - Pará. In: Simpósio de Geologia da Amazônia. Anais... Belém, 13: 1 CD-ROM.
- EMBRAPA. Empresa Brasileira de Pesquisa Agropecuária. 2006. Sistema brasileiro de classificação de solos. 2ª ed., Rio de Janeiro, Embrapa Solos. Centro Nacional de Pesquisa de solos, 306p.
- Fabre, S., Nédélec A., Poitrasson F., Strauss H., Thomazo C. & Nogueira A. 2011. Iron and sulfur isotopes from the Carajás mining province (Pará, Brazil): implications for the oxidation of the ocean and the atmosphere across the archaean-proterozoic transition. *Chemical Geology*, 289: 124-139.
- Feio, G.R.L., Dall'Agnol R., Dantas E.L., Macambira M.J.B., Santos J.O.S., Althoff, F.J. & Soares J.E.B. 2013. Archean granitoid magmatism in the Canaã dos Carajás area: implications for crustal evolution of the Carajás province, Amazonian craton, Brazil. *Precambrian Research*, 227: 157-185.

- Freyssinet Ph., Butt C.R.M. & Morris R.C. 2005. Ore-forming processes related to lateritic weathering. *Econ. Geol. 100th Anniversary*: 681-722.
- Häggi, C., Chiessi, C.M., Merkel, M., Mulitz, S., Prange, M., Schulz, M. & Schefuß, E. 2017. Response of the Amazon rainforest to late Pleistocene climate variability. *Earth and Planetary Science Letters*, 479: 50-59.
- Hallberg J.A. 1984. A geochemical aid to igneous rock identification in deeply weathered terrain. *Journal of Geochemical Exploration*, 20:1-8.
- Hieronymus, B., Kotschoubey, B., Boulègue, J. 2001. Gallium behaviour in some constraining lateritic profiles from Cameroon and Brazil. *Journal of Geochemical Exploration*, 72: 147-163.
- Horbe A.M.C. 1995. *Evolução mineralógica e geoquímica multi-elementar de perfis de solos sobre lateritos e gossans na Amazônia*. Belém, 213p. Tese de Doutorado, Instituto de Geociências, Universidade Federal do Pará.
- Horbe, A.M.C. & Costa, M.L. 2005. Lateritic crust and related soils in eastern Brazilian Amazonia. *Geoderma*, 126: 225-239.
- Huhn, S.R.B., Santos, A.B.S., Amaral, A.F., Ledsham, E.J., Gouveia, J.L., Martins, L.B.P., Montalvão, R.M.G. & Costa, V.G. 1988. O terreno granito-greenstone da região de Rio Maria, Sul do Pará. In: *Proceedings of the 35th Brazilian Geological Congress*. Sociedade Brasileira de Geologia, p. 1438-1453.
- IBGE. Instituto Brasileiro de Geografia e Estatística. 2008. *Mapa de solos do estado do Pará*. 1ª ed., Rio de Janeiro, escala 1:1.800.000.
- João, X.S.J. 2013. Arcabouço geológico-tectônico e implicações metalogenéticas. In: João, X.S.J., Teixeira S.G., Fonseca D.D.F. (eds.). *Geodiversidade do Estado do Pará: Levantamento da geodiversidade*. Belém, Serviço Geológico do Brasil - CPRM, p. 17-21.
- Kotschoubey, B., Calaf J.M.C., Lobato A.C.C., Leite A.A.S. & Azevedo C.H.D. 2005. Caracterização e gênese dos depósitos de bauxita da província de bauxitífera de Paragominas, Noroeste da Bacia do Grajaú, Nordeste do Pará/Oeste do Maranhão. In: Marini Onildo João et al. (orgs.). *Caracterização de depósitos minerais em distritos mineiros da Amazônia*. Brasília, DF, DNPM-CT Mineral, ADIMB, p. 613-698.
- Li, M.Y.H. & Zhou, M.F. 2020. The role of clay minerals in formation of the regolith-hosted heavy rare earth element deposits. *American Mineralogist*, 105: 92-108.
- Mathian, M., Bueno, G.T., Balan, E., Fritsch, E., Nascimento, N.R., Selo, M. & Allard, T. 2020. Kaolinite dating from Acrisol and Ferralsol: A new key to understanding the landscape evolution in NW Amazonia (Brazil). *Geoderma*, 370: 114354.
- Monteiro, H.S., Vasconcelos, P.M.P., Farley, K.A. & Lopes, C.A.M. 2018. Age and evolution of diachronous erosion surfaces in the Amazon: Combining (U-Th)/He and cosmogenic ³He records. *Geochimica et Cosmochimica Acta*, 229: 162-183.
- Morris R.C. & Ramanaidou E.R. 2007. Genesis of the channel iron deposits (CID) of the Pilbara region, Western Australia. *Australian Journal of Earth Sciences*, 54(5): 733-756.
- Nahon, D., Melfi, A. & Conte, C.N. 1989. Présence d'un vieil système de cuirasses ferrugineuses latéritiques em Amazonie du Sud. As transformation in Situ em Latossols Sous la Forêt équatoriale actuelle 308. C.R. Académie des Sciences, Paris, p. 755-760.
- Nahon D.B. 1991. *Introduction to the petrology of soils and chemical weathering*. New York: Wiley-Interscience, 313p.
- Nahon D., Tardy Y. 1992. The Ferruginous Laterites. In: Butt, C.R.M.; Zeegers, H. (eds.). *Regolith, Exploration Geochemistry in Tropical and Subtropical Terrains*. Elsevier Science Publishers, p.41-54.
- Negrão, L.B.A. & Costa, M.L. 2021. Mineralogy and geochemistry of a bauxite-bearing lateritic profile supporting the identification of its parent rocks in the domain of the huge Carajás iron deposits, Brazil. *Journal of South American Earth Sciences*, 108: 103164.

- Oliveira, S.M.B., Trescases, J.J. & Melfi, A.J. 1992. Lateritic nickel deposits of Brazil. *Mineralium Deposita*, 27 (2): 137-146.
- Oliveira S.M.B. & Imbernon R.A.L. 1998. Weathering alteration and related REE concentration in the Catalão I carbonatite complex, central Brazil. *Journal of South American Earth Science*, 11 (4): 379-388.
- Oliveira, M.A., Dall'Agnol, R. & Althoff, F.J. 2006. Petrografia e Geoquímica do Granodiorito Rio Maria da Região de Bannach e comparações com as demais ocorrências. *Revista Brasileira de Geociências*, 36(2): 313-326.
- Ramanaidou E.R., Morris R.C., Horwitz R.C. 2003. Channel iron deposits of the Hamersley Province, Western Australia. *Australian Journal of Earth Sciences*, 50(5): 669-690.
- Rudnick R.L. & Gao S. 2014. The Composition of the Continental Crust. In: Holland H.D & Turekian K.K (eds). *Treatise on geochemistry (Second Edition)*. Oxford, Elsevier-Pergamon. Vol. 4, 1-51 p.
- Schellmann W. 1986. On the geochemistry of laterites. *Chemie der Erde*, 45: 39-52.
- Schellmann W. 1994. Geochemical differentiation in laterite and bauxite formation. *Catena*, 21: 131-143.
- Shuster D.L., Vasconcelos P.M.P., Heim J.A. & Farley K.A. 2005. Weathering geochronology by (U-Th)/He dating of goethite. *Geochim. Cosmochim. Acta*, 69(3), 659-673.
- Silva, A.C.S. & Costa, M.L. 2020. Genesis of the "soft" iron ore at S11D Deposit, in Carajás, Amazon Region, Brazil. *Brazilian Journal of Geology*, 50(1): e20180128.
- Souza, Z.S., Potrel, A., Lafon, J.M., Althoff, F.J., Pimentel, M.M., Dall'agnoL, R. & Oliveira, C.G. 2001. Nd, Pb and Sr isotopes in the Identidade Belt, an Archean greenstone belt of Rio Maria region (Carajás Province, Brazil): implications for the geodynamic evolution of the Amazonia Craton. *Precambrian Research*, 109: 293-315.
- Tardy, Y., Kolbisek B. & Paquet H. 1991. Mineralogical composition and geographical distribution of African and Brazilian periatlantic laterites. The influence of continental drift and tropical palaeoclimates during the past 150 million years and implications for Índia and Australia. *Journal African Earth Sciences*, 12: 283-295.
- Tardy Y. 1997. *Petrology of Laterites and Tropical Soils*. Masson, S.A. Éditeurs, Balkena Publishers, Paris. 408p.
- Taylor S.R. & McLennan S.M. 2001. Chemical composition and element distribution in the earth's crust. *New York, Academic Press*, 2: 697-719.
- Vasquez, M.L., Souza, C.S., Carvalho, J.M.A 2008. *Mapa Geológico e de Recursos Minerais do Estado do Pará*. Belém: CPRM, escala 1:1.000.000.
- Zular, A., Sawakuchi, A.O., Chiessi, C.M., Horta, F.M., Cruz, F.W., Demattê, J.A.M., Ribas, C.C., Hartmann, G.A., Giannini, P.C.F. & Soares, E.A.A. 2019. The role of abrupt climate change in the formation of an open vegetation enclave in northern Amazonia during the late Quaternary. *Global and Planetary Change*, 172: 140-149.